JIPB Journal of Integrative Plant Biology

Research Article
https://doi.org/10.1111/jipb.70184

The HaMYB22–HaGST3.2 module mediates salt stress response in sunflower

Siqi Zhang[1†], Yuliang Han[1†], Qixiu Huang[2†], Weijun Guo[1], Shurui Dong[1], Xinxin Li[1], Qian Zhang[1], Juncheng Zhang[1], Yijun Meng[1], Zhonghua Lei[2], Maohong Cai[1*] and Tao Chen[1*]

1. College of Life and Environmental Sciences, Hangzhou Normal University, Hangzhou 311121, China
2. Institute of Crops Research, Xinjiang Uyghur Autonomous Region Academy of Agricultural Sciences, Urumqi 830000, China
†These authors contributed equally to this work.
*Correspondences: Tao Chen (chentao@hznu.edu.cn, Dr. Chen is fully responsible for distributions of all materials associated with this article); Maohong Cai (caimaohong@hznu.edu.cn)

Siqi Zhang

Tao Chen

ABSTRACT

Soil salinization is a global challenge threatening agricultural production, food security, and sustainable development. As a pioneer crop on saline-alkali land, sunflower plays a crucial role in the improvement and utilization of salt-affected soils. However, the molecular mechanisms underlying sunflower salt tolerance remain poorly understood. In this study, we identified a key R2R3-MYB gene, *HaMYB22*, through a combination of genome and transcriptome analyses. Functional characterization demonstrates that overexpression of *HaMYB22* significantly enhances salt tolerance in both *Arabidopsis* and sunflower, whereas its silencing decreases salt resistance. Protein interaction assays revealed that HaMYB22 interacts with HaMYB120 and HaMYB181. Glutathione S-transferase *HaGST3.2* was identified as a direct target of HaMYB22, and superior haplotype $HaMYB22^{hap1}$ can strongly increase *HaGST3.2* transcripts. Moreover, HaMYB120 and HaMYB181 synergistically strengthen HaMYB22-mediated *HaGST3.2* activation. *HaGST3.2* silencing in sunflower decreases salt tolerance. Our findings revealed the importance of the HaMYB22–HaGST3.2 module in sunflower salt tolerance.

Keywords: *HaMYB22*, ROS, salt tolerance, sunflower

Zhang, S., Han, Y., Huang, Q., Guo, W., Dong, S., Li, X., Zhang, Q., Zhang, J., Meng, Y., Lei, Z., et al. (2026). The HaMYB22–HaGST3.2 module mediates salt stress response in sunflower. J. Integr. Plant Biol. **68:** 1709–1726.

INTRODUCTION

The common sunflower (*Helianthus annuus* L.), an annual herbaceous plant of Asteraceae family, ranks among the world's top three oilseed crops (Lv et al., 2025). This nutritionally valuable crop serves both as an important oil source and as a food product (Harter et al., 2004; Hadidi et al., 2024). As one of the few crops domesticated in North America, sunflower is now widely cultivated around the world (Smith, 2006; Renaut, 2017). Its global cultivation is attributed to remarkable stress tolerance traits, including resistance to barren soils, salt-alkali conditions, drought, and an exceptional capacity for heavy metal absorption, enabling stable yields under diverse environmental stresses worldwide (Badouin et al., 2017; Temme et al., 2020; Liu et al., 2024). Recent investigations have significantly advanced our understanding of sunflower stress resistance mechanisms, particularly in elucidating molecular regulatory networks underlying abiotic stress responses (Manavella et al., 2006; Giacomelli et al., 2012; Gagliardi et al., 2019; Raineri et al., 2022; Leconte et al., 2025).

Salt stress represents a critical constraint on plant growth and agricultural productivity (Kotula et al., 2020; Liang et al., 2024).

This stress triggers primary signaling pathways, including osmotic stress, ionic stress, and secondary oxidative stress (Yang and Guo, 2018). Although reactive oxygen species (ROS) serve as essential components in multiple critical signaling pathways (Nanda et al., 2010; Mittler, 2017), the secondary effects of salt stress induce excessive ROS accumulation, leading to cellular damage through lipid peroxidation, protein denaturation, and nucleic acid degradation, ultimately disrupting metabolic homeostasis (Zhu, 2016; Mittler et al., 2022). To mitigate oxidative damage, plants use a robust enzymatic antioxidant defense system, including superoxide dismutase (SOD), glutathione reductase (GR), and glutathione-S-transferase (GST) (Waszczak et al., 2018; Wang et al., 2024). GST plays a pivotal role in detoxification by conjugating glutathione (GSH) to cytotoxic compounds, thereby neutralizing peroxides and enhancing stress tolerance (Lapenna, 2023; Russell and Richardson, 2023). Both plants and animals can upregulate GST expression under various environmental stresses to modulate cellular redox balance and mitigate oxidative damage (Chen et al., 2017). Studies have shown that the salt stress-responsive gene *SlGSTU4* confers enhanced salt stress tolerance in tomato by reinforcing the ROS scavenging system, significantly enhancing ROS scavenging efficiency (Yuan et al., 2024). PtGSTU17 was identified as a key enzyme responsible for reactive oxygen species elimination in *Poncirus trifoliata* (Zhang et al., 2022b). The cotton glutathione S-transferase GhGSTU17 enhances salt tolerance by improving GST enzymatic activity to facilitate ROS scavenging (Sun et al., 2024).

Transcription factors (TFs) play pivotal roles in maintaining cellular homeostasis under diverse environmental stresses. Among these, the MYB superfamily represents the second largest class of TFs in flowering plant (Wu et al., 2022). Particularly the R2R3–MYB subfamily, as the most extensively characterized and predominant group within the MYB family, has been demonstrated to orchestrate a wide spectrum of physiological processes, metabolic pathways, and stress adaptation mechanisms in plants (Gao et al., 2023; Wu et al., 2024; Bhatt et al., 2025; Zhang et al., 2025). Extensive research has established the regulatory functions of MYB transcription factors in plant salt stress tolerance. In *Arabidopsis*, MYB42 directly binds to the promoter of the *SALT OVERLY SENSITIVE 2* (*SOS2*) gene, facilitating its rapid induction during salt stress (Sun et al., 2020). Similarly, the protein complex formed by OsMYB106, OsSUVH7, and OsBAG4 coordinately regulates *OsHKT1;5* to maintain K^+/Na^+ homeostasis under salt stress conditions in rice (Wang et al., 2020). MdMYB44-like precisely regulates ABA-mediated salt and drought tolerance in apple through the MdPYL8–MdPP2CA signaling module (Chen et al., 2024). Furthermore, SUMOylation of MYB30 under salt stress conditions enhances plant salt tolerance (Gong et al., 2020). The salt-responsive transcription factor AtMYB74 regulates plant salt stress adaptation through the RNA-directed DNA methylation (RdDM) pathway in *Arabidopsis* (Xu et al., 2015; Zhang et al., 2022a). Additionally, the OsMYB2–OsANT1 regulatory module coordinates rice growth and salt tolerance adaptation through the ABA signaling pathway (Nie et al., 2025a). These studies highlight the central role of MYB transcription factors as multifunctional regulators in plant salt stress adaptation through various molecular pathways.

In this study, we used a comprehensive approach combining genome and transcriptomic profiling in sunflower and identified *HaMYB22* as a key gene for salt stress tolerance. Overexpression of *HaMYB22* enhances salt tolerance in *Arabidopsis* and sunflower, while silencing increases sensitivity. HaMYB22 interacts with HaMYB120 and HaMYB181, directly activating *HaGST3.2*. HaMYB120/181 synergistically enhances this activation. Silencing *HaGST3.2* reduces salt tolerance. Our study provides novel insights into the functional mechanisms of MYB transcription factors in sunflower stress adaptation, while also offering valuable genetic resources and a theoretical foundation for improving salt-tolerant sunflower cultivars.

RESULTS

Identification of HaMYB22 as a salt tolerance candidate gene in sunflower

In previous studies, we conducted whole-genome resequencing of 135 natural oil sunflower germplasms and measured the dry weight (DW) of sunflower seedlings, since biomass is considered as a practical measure of salt tolerance (Munns and Tester, 2008). The DW statistical results showed a normal distribution (Figure 1A). Genome-wide association analysis (GWAS) was performed based on this trait (Figure 1B), identifying 75 minor-effect quantitative trait locus (QTLs) that distributed across all 17 sunflower chromosomes, which were annotated to 61 genes. Differential expression genes (DEGs) analysis of the salt stress transcriptome identified three salt-responsive genes, including *HaMYB22* (HanSK08G34500) (Figure 1C; Table S1). Moreover, among 61 candidate gens, 44 genes showed detectable expression. As shown in Figure 1D, the expression levels of 44 genes under salt treatments were normalized and the expression of *HaMYB22* (HanSK08G34500) significantly increased (9.6-fold) after 3 h of NaCl treatment. Further RT-qPCR validation confirmed that *HaMYB22* was strongly induced by salt stress in both roots and leaves across all three developmental stages (germination, seedling stage I, and seedling stage II), with stronger induction in roots than leaves (Figure 1E). Linkage disequilibrium (LD) block analysis was performed on the 18.82 Kb genomic region flanking the *HaMYB22* QTL. As shown in Figure 1F, this LD block contained only *HaMYB22*. Therefore, *HaMYB22* was selected as the key candidate gene for salt stress response.

Overexpression of *HaMYB22* enhanced salt tolerance in *Arabidopsis thaliana*

To evaluate the functional of *HaMYB22* in salt stress adaptation, we expressed the gene in *A. thaliana* (Col-0). To systematically assess the positive seedling efficiency of *HaMYB22*-OE lines, we validated their transcriptional, transformation, and protein accumulation levels through RT-qPCR, positive rate statistics, and Western blot analysis

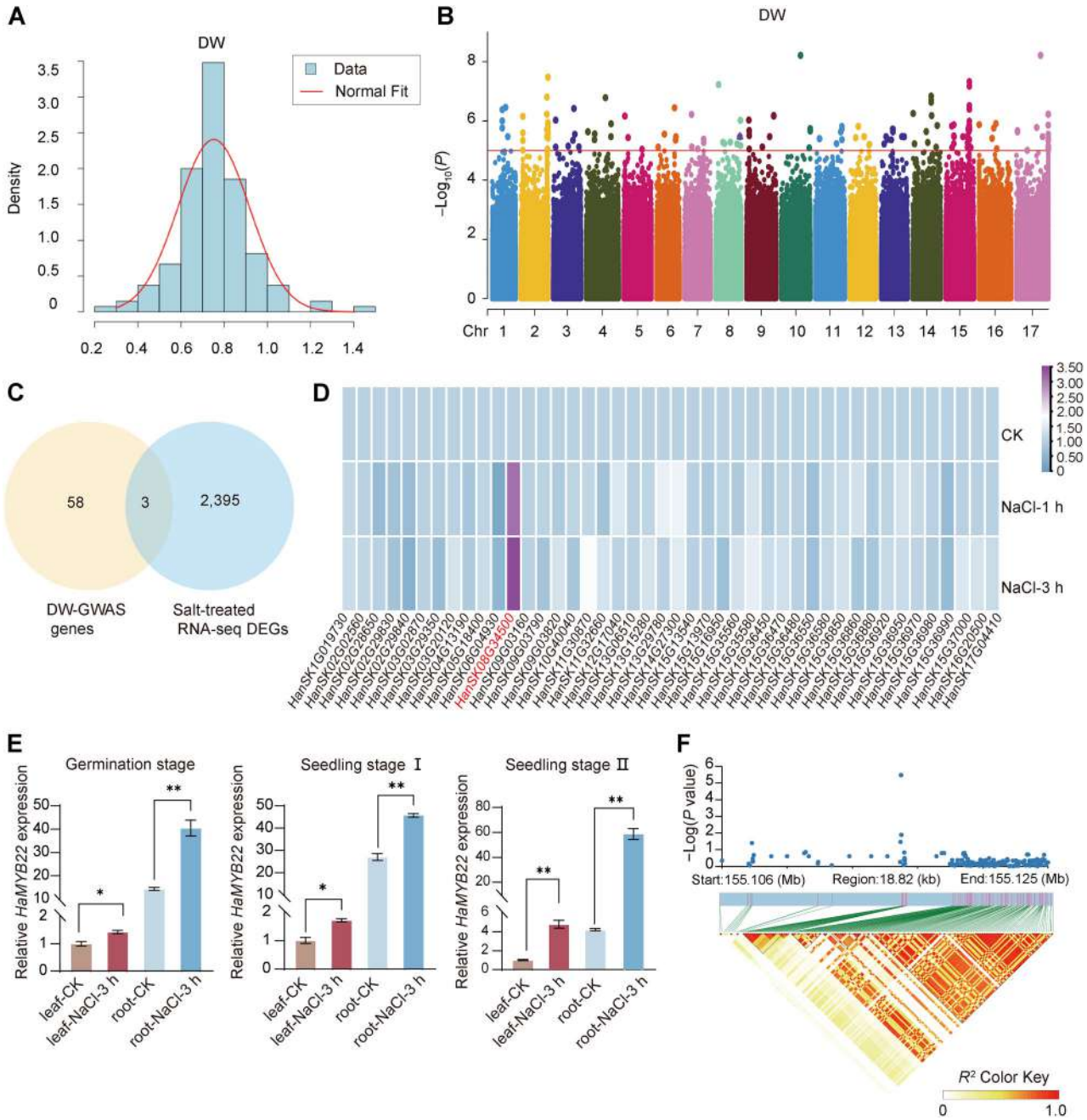

Figure 1. Identification of *HaMYB22* as a salt-regulatory candidate gene

(A) Normal distribution of dry weight (DW) phenotypes in the sunflower association panel ($n = 135$). **(B)** Genome-wide association study (GWAS) Manhattan plot for DW. Each point represents an single-nucleotide polymorphism (SNP), where the x-axis denotes chromosomal coordinates and the y-axis represents $-Log_{10}(P\text{-value})$ magnitudes. The red line indicates the significance threshold ($-Log_{10}(P) \geq 5$). **(C)** Integration of GWAS candidate genes (yellow) and salt stress-responsive differentially expressed genes (DEGs, blue). Overlapping genes represent high-priority candidates. **(D)** Heatmap of expression patterns for candidate salt stress-responsive genes within the quantitative trait locus (QTL). 44 genes with detectable transcriptional expression were visualized. **(E)** RT-qPCR validation of *HaMYB22* transcript levels in roots and leaves under salt stress at three developmental stages (germination, seedling stage I, and seedling stage II). Data are presented as means ± *SD* ($n = 3$ biological replicates) normalized to *HaTubulin* (**$P < 0.01$; Student's *t*-test). **(F)** Linkage disequilibrium (LD) plot for SNPs in the 155.106 to 155.125 Mb region surrounding the *HaMYB22*. The color key represents linkage disequilibrium values (R^2).

(Figure S1). Under control conditions, two independent *HaMYB22*-overexpressing (OE) lines (#3 and #5) showed no phenotypic divergence from wild-type plants (Figure 2A). However, under NaCl treatments of 90 and 150 mM, *HaMYB22*-OE lines showed significantly enhanced salt tolerance (Figure 2B, C), characterized by both lateral root length and lateral root number. Quantitative analysis revealed that *HaMYB22*-OE lines developed 45% and 100% longer lateral roots (Figure 2D, E) and produced 1.8- and 3.3-fold more lateral roots compared to Col-0 under 90 and 150 mM

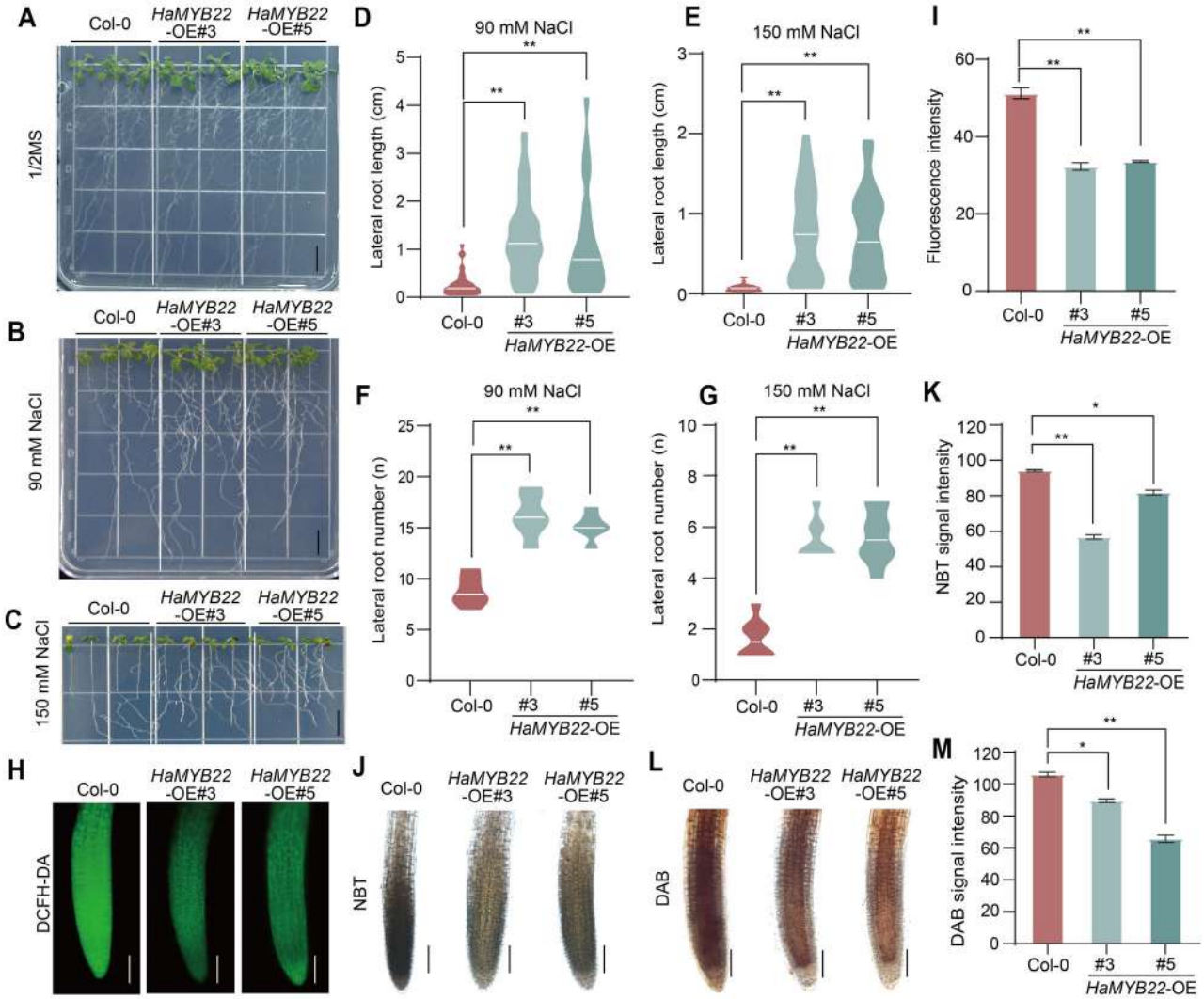

Figure 2. Overexpression of *HaMYB22* improves salt tolerance in *Arabidopsis thaliana*

(A–C) Representative images of salt tolerance analysis for wild-type (Col-0) and two independent *HaMYB22*-OE lines (#3, #5). Five-day-old seedlings with approximately 1-cm-long hypocotyls were transferred from Murashige and Skoog (MS) medium to the 1/2MS medium **(A)**, 1/2MS medium supplemented with 90 mM NaCl **(B)**, and supplemented with 150 mM NaCl **(C).** Seedlings grown on 1/2MS medium **(A)** served as the control group. Photographs were taken 7 d after transfer. Scale bars = 1 cm. Each treatment was performed by three independent biological replicates. **(D–G)** Quantification of lateral root length **(D)**, lateral root number **(E)** under 90 mM NaCl treatment and lateral root length **(F)**, and lateral root number **(G)** under 150 mM NaCl treatment. Fifteen seedlings per genotype from three independent biological replicates were examined in each treatment. ($n = 12$, $^{**}P < 0.01$, Student's *t*-test). **(H–M)** Representative histochemical staining and quantitative analysis of single-nucleotide polymorphism (ROS) in Col-0 and *HaMYB22*-OE lines under 150 mM NaCl treatment for 3 h. General ROS level detected by DCFH-DA staining **(H)** and its quantification **(I)**. Superoxide ($O_2{\bullet}^-$) visualized by NBT staining **(J)** and its quantification **(K)**. H_2O_2 accumulation shown by DAB staining **(L)** and its quantification **(M)** (Scale bar = 100 μm, $n = 12$, $^{**}P < 0.01$; Student's *t*-test) ($^{**}P < 0.01$; Student's *t*-test) ($n = 6$, $^{*}P < 0.05$, $^{**}P < 0.01$, Student's *t*-test). DCFH-DA fluorescence was detected and recorded using conventional fluorescence microscopy, while DAB and NBT staining patterns were observed and imaged through stereomicroscopy.

NaCl treatment (Figure 2F, G). These dose-dependent morphological modifications suggest that *HaMYB22* plays a crucial role in root system adaptation to saline environments. Therefore, heterologous expression of *HaMYB22* in *Arabidopsis* can alleviate salt-sensitive phenotypes and significantly enhance plant salt tolerance.

Salt stress triggers secondary oxidative damage through accumulation of reactive oxygen species (ROS). To assess whether *HaMYB22* modulates this oxidative component, we compared ROS accumulation in Col-0 and transgenic lines under 150 mM NaCl treatment. After 3 h of salt exposure, histochemical analysis revealed substantially stronger staining for superoxide ($O_2{\bullet}^-$; NBT) and hydrogen peroxide (H_2O_2; DAB and DCFH-DA) in Col-0 compared to *HaMYB22*-OE lines, and quantitative analysis confirmed this visual (Figure 2H–M). This attenuated oxidative burst in *HaMYB22*-OE plants demonstrated *HaMYB22*'s capacity to decrease salt-induced ROS damage.

Silencing of *HaMYB22* reduces salt tolerance in sunflower

To study the effect of *HaMYB22* on sunflower under NaCl stress, silencing of *HaMYB22* was performed using a tobacco rattle virus (TRV)-based VIGS system. RT-qPCR confirmed effective silencing, with residual salt-induced expression remaining lower than EV (> 70% reduction in *HaMYB22* transcripts) (Figure 3A). Under normal conditions, 14-day-old Vi: *HaMYB22* seedlings showed no developmental differences versus empty vector (EV) controls (Figure S2). Under 200 mM NaCl treatment, expression of *HaMYB22* was strongly upregulated in both leaves and roots of EV and Vi: *HaMYB22* lines (Figures 3A, S3), and Vi: *HaMYB22* lines showed pronounced hypersensitivity to 200 mM NaCl in leaves.

Within 12 h of salt stress, Vi: *HaMYB22* plants displayed accelerated leaf damage (Figure 3B). For quantitative assessment of injury severity, a four-category classification system of salt-induced leaf damage was used based on progressive tissue compromise. Leaves that showed minimal symptomology (< 10% affected area) were designated category I, while moderate damage manifesting as 33%–50% leaf curling defined category II. Category III represented severe impairment with approximately 75% structural compromise, and

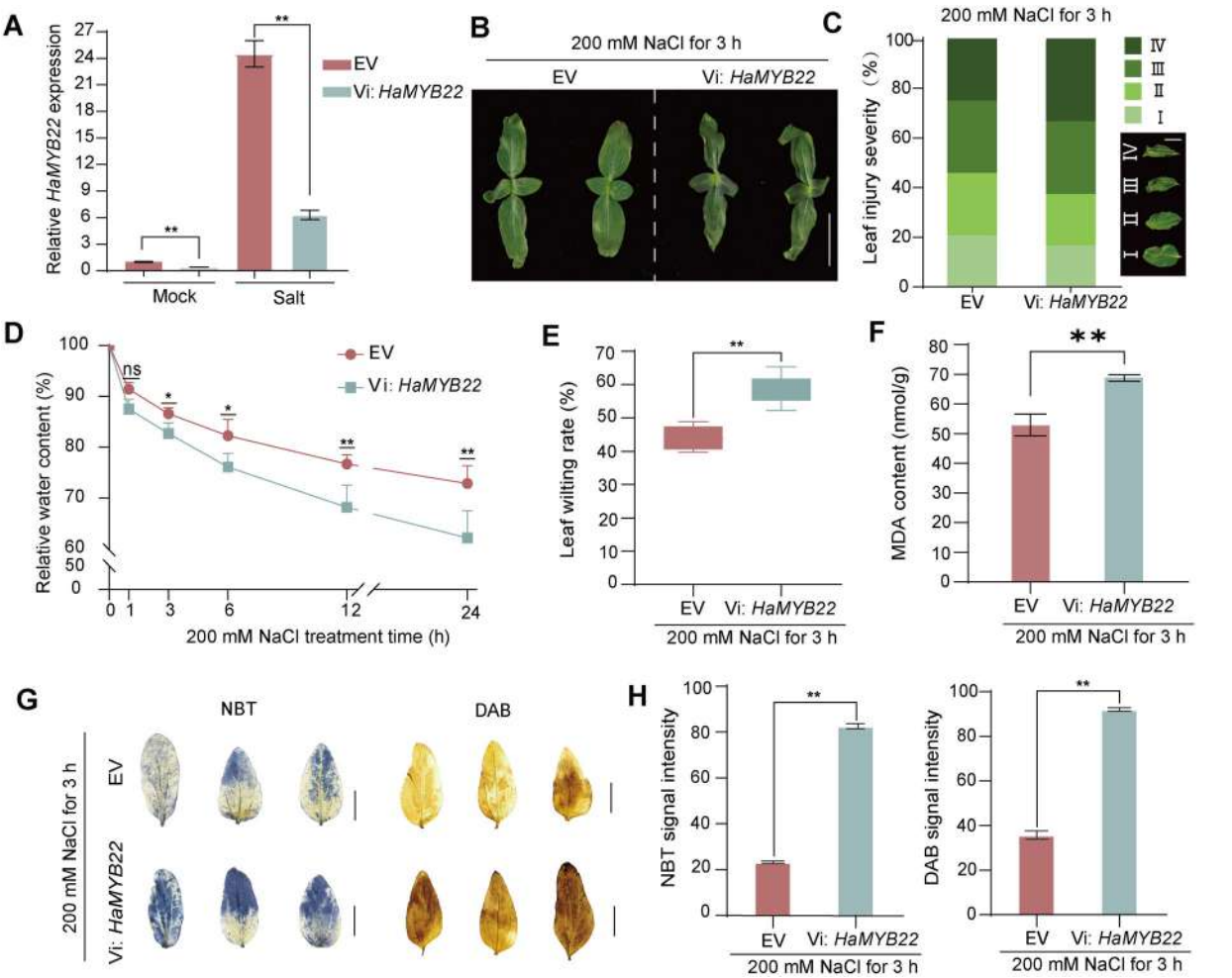

Figure 3. *HaMYB22* silencing compromises salt tolerance in sunflower

(A) Relative expression of *HaMYB22* in 14-day-old sunflower seedlings expressing empty vector (EV) and *HaMYB22*-silencing construct (Vi: *HaMYB22*) under mock (untreated) and salt (200 mM NaCl, 3 h) conditions, with *HaTubulin* as the endogenous control ($n = 3$, $^{**}P < 0.01$; Student's *t*-test). **(B, C)** Representative phenotypes **(B)** and quantitative assessment of salt-induced leaf damage **(C)** in EV and Vi: *HaMYB22* plants following 3 h exposure to 200 mM NaCl (Scale bar = 2.5 cm). Two-week old seedlings grown in 1/5 Hoagland liquid medium were transferred to the same medium containing 200 mM NaCl. Tissue deterioration was classified into four severity categories (I: intact → IV: necrotic). Leaf damage severity in EV and Vi: *HaMYB22* plants was statistically analyzed after a 3 h 200 mM NaCl treatment. **(D)** Relative water content (RWC) from detached leaves of EV and Vi: *HaMYB22* after 200 mM NaCl treatment ($n = 12$, $^{*}P < 0.05$, $^{**}P < 0.01$; Student's *t*-test). Whole-seedling fresh weight was measured at 1, 3, 6, 12, and 24 h after NaCl treatment, and RWC was calculated accordingly. **(E)** Leaf wilting rate calculated from the ratio of the pre-treated single leaf area to the treated leaf area after a 3 h of 200 mM NaCl treatment in EV and Vi: *HaMYB22* plants ($n = 12$, $^{**}P < 0.01$; Student's *t*-test). **(F)** Membrane damage of EV and Vi: *HaMYB22* assessed by MDA content following a 3 h 200 mM NaCl treatment ($n = 3$, $^{**}P < 0.01$; Student's *t*-test). **(G–H)** Representative histochemical detection **(G)** and quantification **(H)** for superoxide (NBT) and hydrogen peroxide (DAB) after a 3 h 200 mM NaCl exposure in EV and Vi: *HaMYB22* plants (Scale bar = 1.0 cm, $n = 12$, $^{**}P < 0.01$; Student's *t*-test).

category IV indicated complete physiological collapse characterized by 100% leaf shrinkage and irreversible cellular damage. As shown in Figure 3C, *HaMYB22*-silenced plants showed a significant increase in irreversibly damaged leaves (category IV) compared to controls. Vi: *HaMYB22* showed lower relative water content (RWC) from 1 h, persisting throughout the 24 h treatment (Figure 3D). NaCl treatment causes osmotic stress in plants, leading to leaf water loss and wilting. Notably, Vi: *HaMYB22* displayed exacerbated wilting symptoms, showing a 32.6% greater reduction in leaf area compared to EV (Figure 3E).

Malondialdehyde (MDA), a key byproduct of membrane lipid peroxidation and a well-established biomarker of oxidative stress (Gill and Tuteja, 2010), was quantified under salt stress conditions. Vi: *HaMYB22* plants accumulated significantly higher MDA levels compared to EV (Figure 3F), demonstrating more severe oxidative damage to membrane lipids. To examine the accumulation of ROS under salt stress, we used staining assays of NBT and DAB in EV and Vi: *HaMYB22* plants under 200 mM NaCl treatment for 3 h. Both NBT and DAB staining both showed that the active oxygen burst in the leaves and roots of Vi: *HaMYB22* was stronger than EV, indicating that $O_2\bullet^-$ and H_2O_2 were highly accumulated in Vi: *HaMYB22* (Figures 3G, H, S3C, D). Collectively, *HaMYB22* silencing compromised salt tolerance in sunflower by elevating ROS accumulation and exacerbating oxidative cellular damage.

Transient overexpression of *HaMYB22* enhances salt tolerance in sunflower

To investigate the effect of *HaMYB22* overexpression on sunflower salt stress tolerance, we engineered transient overexpression constructs in two-leaf-stage sunflower seedlings, expressing *HaMYB22*-FLAG (designated *HaMYB22*-OE) alongside GFP-expressing controls (EV). Following a three-day establishment period, acute exposure to 300 mM NaCl revealed striking phenotypic divergence. Within 1 h, EV controls showed pronounced wilting, while *HaMYB22*-OE maintained leaf integrity (Figure 4A). Western blot analysis confirmed robust expression of both transgenes (Figure 4B), establishing the experimental platform for functional assessment.

Quantitative evaluation using our established damage severity metric demonstrated that *HaMYB22*-OE plants predominantly sustained category I-II damage (Figure 4C). Statistical results of RWC in EV and *HaMYB22*-OE within 24 h after 300 mM NaCl treatment also confirmed this phenomenon (Figure 4D). The RWC of EV was significantly lower than that of *HaMYB22*-OE after 3 h of NaCl treatment, and this pattern persisted throughout the 24 h stress period. By measuring leaf area before and after NaCl treatment, *HaMYB22*-OE showed only a 40% reduction in leaf area, while EV showed over 50% reduction, demonstrating more severe leaf wrinkling in EV under salt stress (Figure 4E).

To evaluate ROS-induced lipid peroxidation in cell membranes under salt stress, we quantified the MDA content following a 1 h exposure to 300 mM NaCl. As depicted in Figure 4F, *HaMYB22*-OE showed a significantly reduced MDA concentration compared to the control, implying enhanced protection against membrane lipid damage. Consistent with this, NBT and DAB staining revealed markedly weaker signals for $O_2\bullet^-$ and H_2O_2, respectively, in *HaMYB22*-OE plants relative to EV controls (Figure 4G, H). This reduction in ROS accumulation was also observed specifically in roots under the same stress conditions (Figure S4). The observed decrease in ROS in *HaMYB22*-OE sunflower roots aligns with the trend previously detected in Arabidopsis *HaMYB22*-OE lines (Figure 2). Taken together, these findings indicate that *HaMYB22* enhances plant salt tolerance by negatively regulating ROS accumulation, and this function is conserved between *Arabidopsis* and sunflower.

In conclusion, the improvement of *HaMYB22*-OE in salt tolerance is corroborated by the salt-sensitive phenotype observed upon silencing of *HaMYB22*, underscoring the role of *HaMYB22* as a positive regulator in sunflower's adaptive response to salinity.

HaMYB22 encodes a conserved R2R3 domain transcription factor

To examine HaMYB22 subcellular localization, the HaMYB22–GFP construct was transformed into sunflower protoplasts and tobacco leaves. HaMYB22 predominantly localized to the nucleus in both sunflower protoplasts (Figure 5A) and tobacco leaves (Figure 5B).

To further explore the expression pattern of *HaMYB22* in sunflower, RT-qPCR was performed across different developmental stages and tissues, as schematically illustrated in Figure 5C. *HaMYB22* expression was detected at all developmental stages, with elevated levels observed in cotyledons during germination, in hypocotyls at seedling stage I, in leaves at seedling stage II, and in primary and lateral roots during the flowering stage (Figure 5C). These findings suggest that HaMYB22 may play diverse roles across different developmental phases in sunflower.

To assess the transcriptional activation activity of HaMYB22, we cloned the full-length coding sequence into the pGBKT7 vector and expressed it in yeast. The full-length HaMYB22 protein possesses self-activation activity. To identify the specific activation domain, the HaMYB22 was divided into the N-terminal region containing the R2R3 domain (HaMYB22-N) and the C-terminal region (HaMYB22-C) (Figure 5D). Only the C-terminal fragment retained strong self-activation, whereas the R2R3-containing N-terminal fragment showed no activity (Figure 5E). Yeast two-hybrid (Y2H) assays further revealed that HaMYB22 can form homodimers through the R2R3 domain (Figure 5E). Together, these data indicate that the transcriptional activation function of HaMYB22 resides in its C-terminal region, while the R2R3 domain is essential for protein dimerization.

HaMYB22 as a central hub in the R2R3–MYB family salt stress signaling network

To investigate other salt stress-responsive genes among sunflower R2R3–MYB family members, transcriptome data,

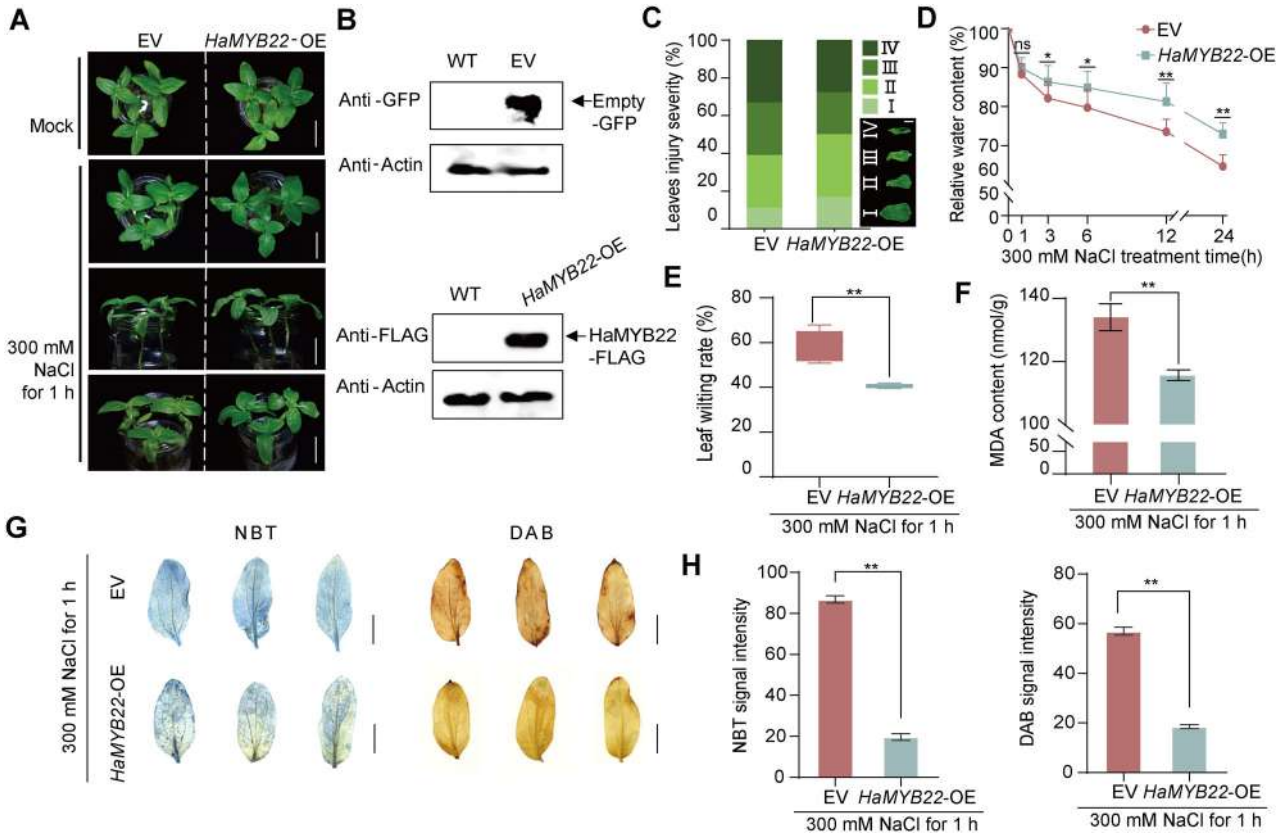

Figure 4. Overexpression of *HaMYB22* in sunflower enhanced plant salt tolerance

(A) Representative phenotypes of sunflower lines expressing empty vector GFP (EV) and the *HaMYB22*-overexpressing construct (*HaMYB22*-OE) before and after 300 mM NaCl treatment (Scale bars = 2.5 cm). Seedlings cultured in 1/5 Hoagland liquid medium were exposed to 300 mM NaCl prepared in the same basal medium. **(B)** Immunoblot validation of EV and *HaMYB22*-OE transformed sunflower materials 3 d after transformation. WT was used as a negative control, *HaMY22*-OE was detected using an anti-FLAG antibody, EV was monitored with an anti-GFP antibody, and actin was used as the loading control**. (C)** Statistical analysis of leaf damage in EV and *HaMYB22*-OE plants after a 1 h treatment with 300 mM NaCl. The damaged leaves were classified into four progressive categories based on tissue deterioration. **(D)** RWC from detached leaves of EV and *HaMYB22*-OE after 300 mM NaCl treatment ($n = 12$, $^{*}P < 0.05$, $^{**}P < 0.01$; Student's *t*-test). Fresh biomass measurements of entire seedlings were conducted at specified intervals (1, 3, 6, 12, and 24 h) following salinity stress initiation, enabling subsequent computation of RWC. **(E)** Leaf wilting rate calculated from the ratio of the pre-treated single leaf area to the salt-treated leaf area under a 1 h 300 mM NaCl treatment ($n = 12$, $^{**}P < 0.01$; Student's *t*-test). **(F)** MDA content of EV and *HaMYB22*-OE plants after 300 mM NaCl treatment for 1 h ($n = 3$, $^{**}P < 0.01$; Student's *t*-test). **(G–H)** Representative histochemical staining **(G)** and quantification **(H)** of superoxide (NBT) and hydrogen peroxide (DAB) accumulation in EV and *HaMYB22*-OE plants under a 1 h 300 mM NaCl treatment (Scale bar = 1.0 cm, $n = 12$, $^{**}P < 0.01$; Student's *t*-test).

comprising sunflower root and leaf tissues subjected to NaCl treatment, were analyzed. Five R2R3–MYB genes, *HaMYB2*, *HaMYB22*, *HaMYB120*, *HaMYB173*, and *HaMYB181* showed strong responses to NaCl, with heatmap analysis highlighting their induction, particularly in root tissues (Figure 6A). Promoter analysis of these genes revealed the presence of salt-responsive cis-elements, including ABRE, TC-rich, and MBS motifs (Figure S5A). To validate the transcriptomic findings, RT-qPCR was conducted, revealing distinct expression profiles among the HaMYBs under salt stress (Figure S5B).

Functional analysis of HaMYBs under NaCl stress was further explored through heterologous expression in prokaryotes. *E. coli* expressing pET-32α-HaMYBs showed significantly enhanced growth than pET-32a controls (Figure 6B), demonstrating that heterologous expression of *HaMYBs* increased salt resistance. These results confirm their positive regulatory roles as transcription factors in the salt stress responses.

To validate the interactions among these salt-responsive HaMYB proteins, yeast two-hybrid assays were first performed. All proteins showed strong transcriptional activation activity, except HaMYB2 with weak activity (Figure S6A). Consistent with our previous results, the N-terminal sequences containing the R2R3 domains from these HaMYBs were cloned into pGBKT7 and showed no self-activation activity (Figure S6B). The Y2H assay revealed distinct dimerization patterns (Figure 6C). Specifically, HaMYB22, HaMYB120, and HaMYB173 formed stable homodimers, whereas HaMYB2 and HaMYB181 engaged exclusively in heterodimeric interactions. Notably, HaMYB22 emerged as a network hub, participating in both homodimeric and heterodimeric interactions with HaMYB120 and HaMYB181, suggesting its central regulatory role in salt stress signaling.

Further validation of interactions between HaMYB22 and HaMYB120/HaMYB181 was achieved through luciferase

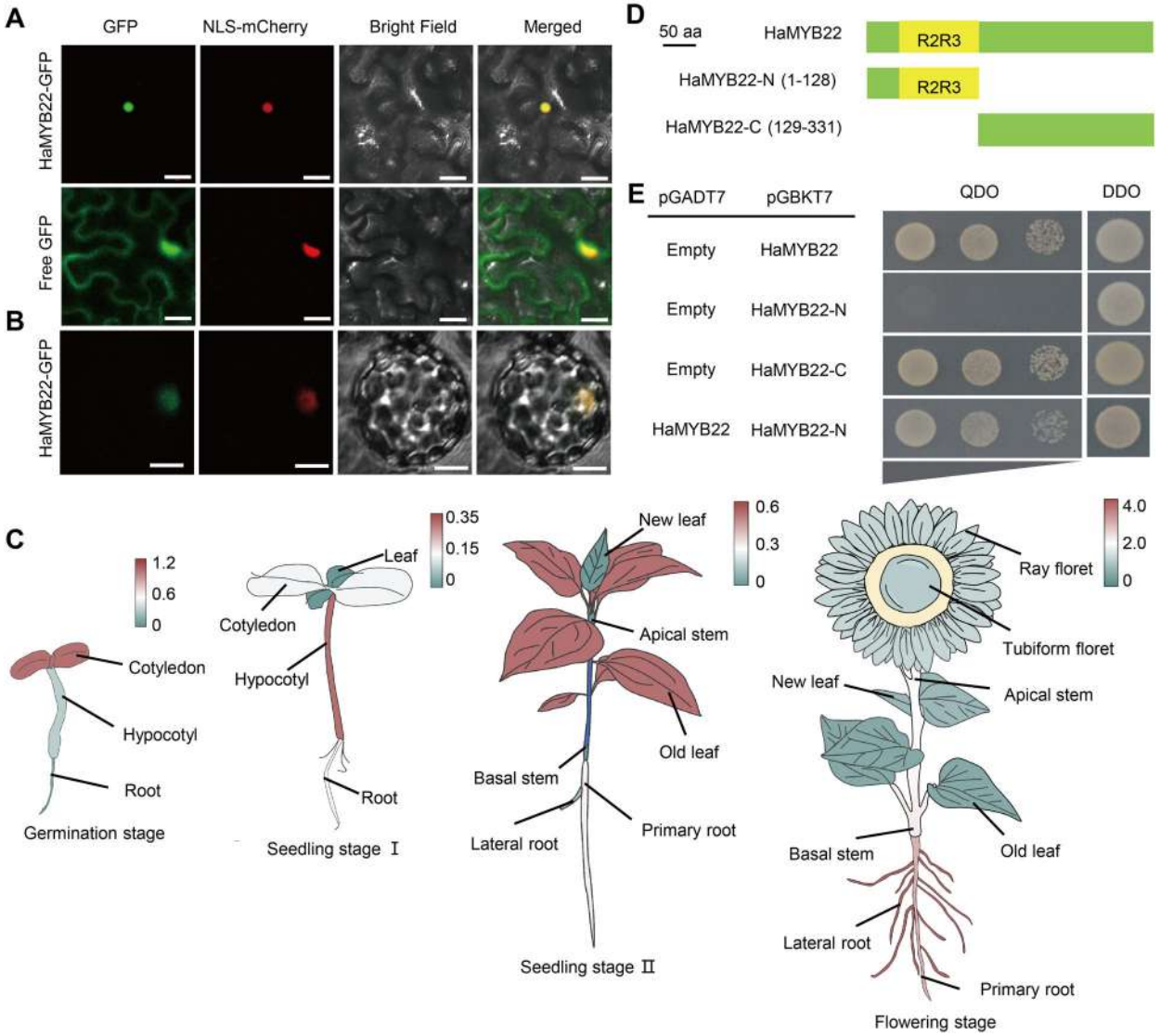

Figure 5. Functional characterization of *HaMYB22*

(A, B) Subcellular location of HaMYB22 in leaf epidermal cells of *Nicotiana benthamiana* **(A)** and sunflower leaf protoplasts **(B)**. NLS–mCherry was used as a nucleus marker. Free GFP was used as a control. Fluorescence signals were acquired through confocal microscopy (LSM710). Scale bars = 10 μM. **(C)** Spatiotemporal expression profiling of *HaMYB22* in various periods and tissues of sunflower. Gene expression levels of *HaMYB22* were quantified by RT-qPCR analysis in distinct developmental phases: germination stage, seedling stage I, seedling stage II, and flowering stage across various tissues. Expression patterns were visualized using TBtools software and illustrated through schematic diagrams for intuitive representation. Data represent means ± *SD* of three biological replicates normalized to the reference gene. *HaTubulin* was used as the endogenous control gene. **(D)** Schematic diagram of *HaMYB22*. The N-terminal represents 1–128 amino acids containing the R2R3 domain (yellow); the C-terminal represents the remaining 129–331 amino acids (green). **(E)** Self-interaction of *HaMYB22* detected by the yeast two-hybrid (Y2H) assay. Both the full-length and C-terminal regions of HaMYB22 show transcriptional activity. QDO: SD/−His/−Leu/−Trp/−Ade, quadruple dropout medium. DDO: SD/−Leu/−Trp, double dropout medium. The triangle in the figure indicates yeast concentration gradients.

complementation imaging (LCI) and bimolecular fluorescence complementation (BiFC) assays *in vivo* (Figure 6D, E), as well as pull-down assays *in vitro* (Figure 6F, G). These findings collectively establish HaMYB22 as a pivotal regulator within the MYB family, orchestrating salt stress responses.

HaMYB22 binds to the promoter of *HaGST3.2*

To elucidate the salt-responsive signaling pathway mediated by *HaMYB22* in sunflower, the samples from both EV and *HaMYB22*-OE plants before 300 mM NaCl treatment and 3 h post-treatment were collected for transcriptome sequencing analysis. Five candidate downstream target genes (*HaLacs1*, *HaLEA46*, *HaLTP*, *HaGST3.1*, and *HaGST3.2*) all contain MYB binding sites in their promoters (Figure S7A), which were significantly induced by both HaMYB22 and NaCl treatment, as visualized in the expression heatmap (Figure S7B). Further validation via RT-qPCR in EV and Vi: *HaMYB22* confirmed that all five genes were down-regulated in *HaMYB22*-silencing plants but displayed distinct expression patterns under salt stress (Figure S7C), supporting their role as downstream targets of *HaMYB22* in the salt stress response pathway.

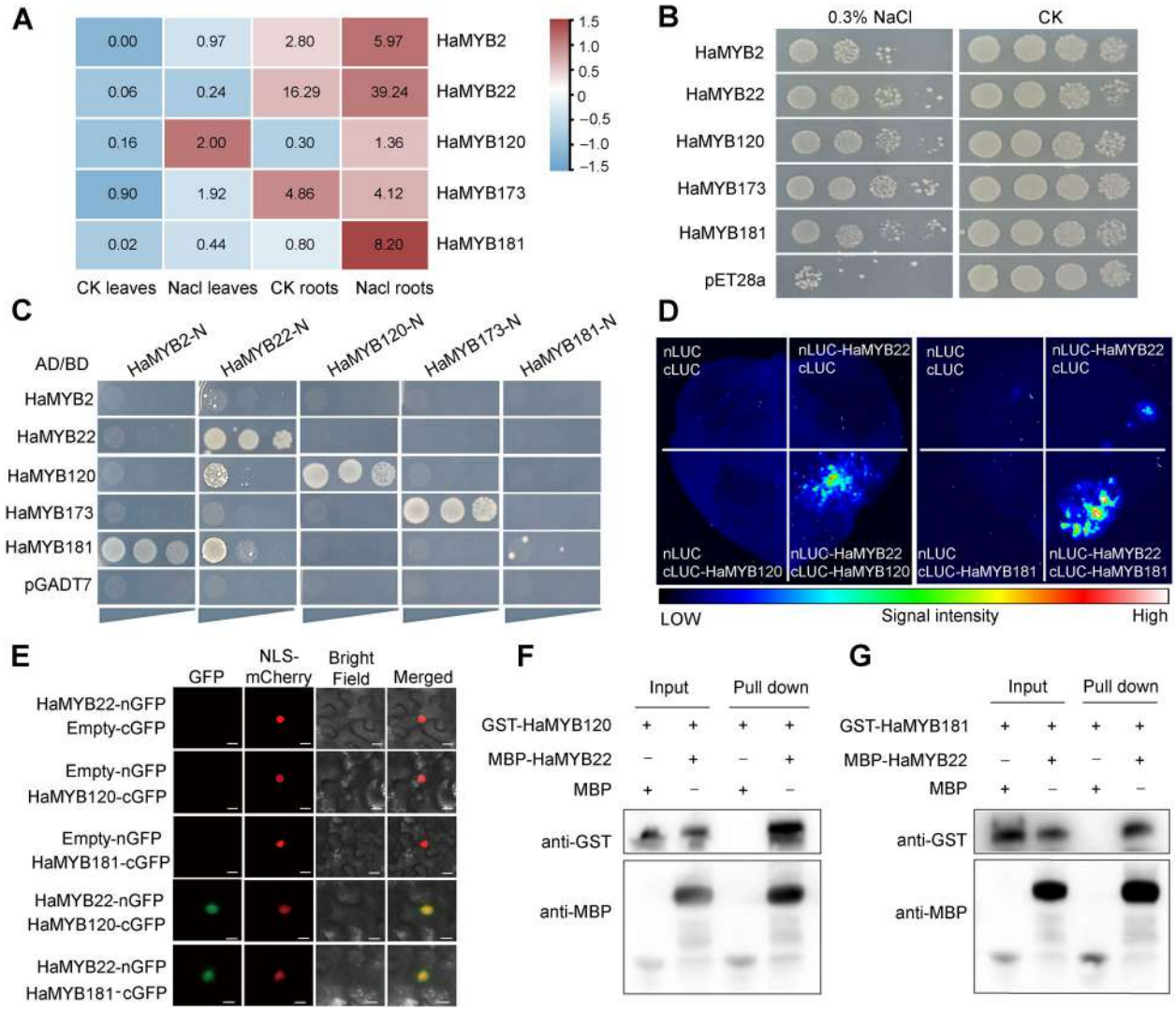

Figure 6. Identification and interaction network analysis of salt-responsive R2R3-MYB transcription factors

(A) Heatmap analysis of NaCl strongly responsive genes in the sunflower R2R3–MYB family before and after NaCl treatment in leaf and root tissues. Color gradient indicates expression levels normalized by *Z*-score transformation. Hierarchical clustering reveals tissue-specific and NaCl-induced expression dynamics. **(B)** Salt stress assay of *E. coli* harboring pET-32α and pET-32α-MYBs. Bacterial suspensions containing pET-32α and pET-32α-MYB proteins were placed on LB solid medium supplemented with 0.3% NaCl and 0.1 mM IPTG, with medium lacking both NaCl and IPTG serving as the control (CK). The cell cultures were diluted with LB medium to different proportions (10°, 10^{-1}, 10^{-2}, and 10^{-3}). **(C)** Y2H assay for interaction verification among R2R3–MYB proteins. Interaction was determined by yeast growth on the QDO medium. Triangles in the figure indicate yeast concentration gradients. **(D)** The LCI assay validated the interaction between HaMYB22 with HaMYB120 and HaMYB181. The indicated combinations of constructs were transfected into *Nicotiana benthamiana* leaves and the luciferase activity was detected 3 d after infiltration. The color gradient represents the relative intensity of the luciferase signal provided by the cooled CCD camera. All experiments were repeated three times, with similar results. **(E)** Interaction of HaMYB22 with HaMYB120 and HaMYB181 validated by the BiFC assay *in vivo*. NLS–mCherry was used as a nucleus marker. The combination of HaMYB22-nGFP and Empty-cGFP was used as a negative control. The fluorescence signal was detected using an LSM710 confocal microscope. **(F, G)** *In vitro* pull-down assay validates the interaction of HaMYB22 with HaMYB120 **(F)** and the interaction of HaMYB22 with HaMYB181 **(G)** MBP-HaMYB22 fusion protein was incubated with GST-HaMYB120 or GST-HaMYB181 in amylose resin, while control groups containing GST-HaMYB120 or GST-HaMYB181 with MBP-tag alone served as negative controls. The input proteins and the eluate protein were subjected to immunoblot assays using the antibodies specified in the figure. The symbols "−" and "+" represent the absence and presence of the corresponding proteins, respectively.

Yeast one-hybrid (Y1H) assays were performed to identify the direct target of HaMYB22. HaMYB22 showed specific binding to the *HaGST3.2* promoter in Y1H assays, indicating direct transcriptional regulation (Figure 7A). To precisely locate the HaMYB22-binding fragment within the *HaGST3.2* promoter, the 2,000 bp sequence was divided as illustrated in Figure 7B. Y1H assays further demonstrated specific binding of HaMYB22 to the F4 fragment (Figure 7C) and the F4.4 fragment (Figure 7D) of the *HaGST3.2* promoter. Based on Y1H findings, subsequent EMSA was performed using biotin-labeled probes (P1/P2) derived from this 80 bp region. Purified MBP–HaMYB22 fusion protein formed shifted bands with both probes, and the signal intensity decreased competitively with unlabeled probes (Figure 7E), confirming sequence-specific DNA binding *in vitro*. To further validate the regulatory relationship, RT-qPCR analysis was performed in Vi:

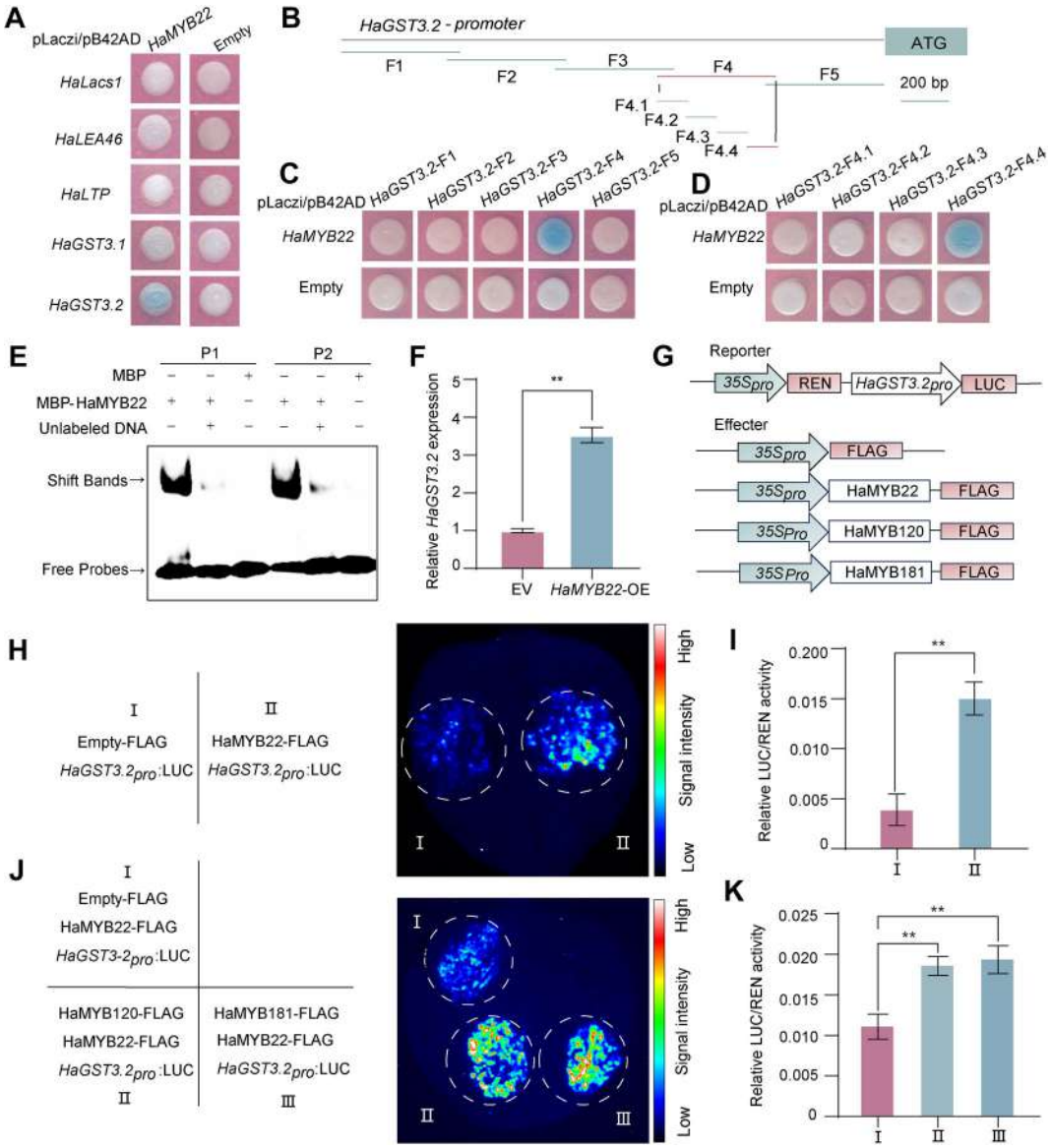

Figure 7. HaMYB22 directly binds to the promoter of *HaGST3.2* and activates its expression

(A) HaMYB22 binds to the promoter of *HaGST3.2* confirmed by the yeast one-hybrid (Y1H) assay. The effector construct pB42AD-HaMYB22 was introduced into the EGY48 yeast strain along with a series of reporter plasmids containing promoters of *HaLacs1*, *HaLEA46*, *HaLTP*, *HaGST3.1*, and *HaGST3.2* fused to the pLacZi vector. Transformants were initially selected on SD/−Trp/−Ura medium, followed by incubation on SD/−Trp/−Ura/Gal/Raf/X-Gal plates at 30°C, to assess β-galactosidase activity through blue pigment production. **(B)** Structure of the *HaGST3.2* promoter region (2,000 bp upstream of the ATG initiation codon). The full length is divided into five segments of 400 bp, and the P4 segment is divided into four segments of 80 bp. **(C, D)** Y1H assay validating the interaction of HaMYB22 on the *HaGST3.2* promoter. HaMYB22 directly binds to **(C)** F4 and **(D)** F4.4 of the *HaGST3.2* promoter. Positive transformants were primarily screened on SD/−Trp/−Ura selection medium and subsequently cultured on SD/−Trp/−Ura/Gal/Raf/X-Gal indicator plates at 30°C for visual detection of β-galactosidase activity via blue chromogenic development. **(E)** The EMSA assay shows that HaMYB22 directly binds to the promoter fragments of *HaGST3.2*. The labeled *HaGST3.2* promoter fragments P1 and P2 were incubated with MBP–HaMYB22 fusion protein, with control groups containing the same labeled fragments with the MBP-tag alone serving as negative controls. The unlabeled probes were used as competitors. The symbols "+" and "−" indicate the presence or absence of corresponding probes and proteins, respectively. **(F)** RT-qPCR quantification of *HaGST3.2* transcript levels in *HaMYB22*-OE plants (***P* < 0.01; Student's *t*-test). **(G)** The structure diagram of the reporters and effectors. $HaGST3.2_{pro}$ represents the upstream 2,000 bp promoter sequences of *HaGST3.2*. **(H)** Transient luciferase assay shows that HaMYB22 can promote the expression of *HaGST3.2*. The effector construct *35S: HaMYB22-FLAG* and the reporter plasmid *35S: REN-proHaGST3.2: LUC* were co-delivered into *Nicotiana benthamiana* leaves through agrobacterium-mediated transient expression. The construct combination of *35S: FLAG* and *35S: REN-proHaGST3.2: LUC* served as the control. The color gradient represents the relative intensity of the luciferase signal provided by the cooled CCD camera. **(I)** The relative luciferase activity (firefly LUC normalized to Renilla REN) of the *HaGST3.2* promoter in response to HaMYB22 was measured, with the empty FLAG vector serving as the control group ($n = 4$, ***P* < 0.01; Student's *t*-test). **(J)** The transient luciferase assay shows that the interaction between HaMYB22 with HaMYB120 and HaMYB181 promotes the expression of *HaGST3.2*. The color gradation reflects variations in luciferase signal intensity as detected by the cooled CCD imaging system. **(K)** The relative reporter activity (firefly luciferase/Renilla luciferase) in response to the interaction between HaMYB22 and HaMYB120 or HaMYB181 was measured. Expression was significantly enhanced compared to the HaMYB22-FLAG control ($n = 4$, ***P* < 0.01; Student's *t*-test).

HaMYB22 plants. The result showed that *HaGST3.2* transcript levels were significantly downregulated in Vi: *HaMYB22* plants (Figure 7F), confirming that *HaMYB22* positively regulates *HaGST3.2* expression *in vivo*. For *in vivo* validation, dual-luciferase assays were performed in *Nicotiana* leaves by co-transforming with reporter construct $HaGST3.2_{pro}$: LUC and effectors plasmid *HaMYB22*-FLAG or an empty FLAG vector (Figure 7G). HaMYB22 significantly enhanced the activity of $HaGST3.2_{pro}$-driven luciferase (Figure 7H, I), confirming the transcriptional activation role of HaMYB22 on *HaGST3.2*.

To investigate the synergistic effect of the interaction between HaMYB22, HaMYB120, and HaMYB181 proteins on HaMYB22-mediated regulation of *HaGST3.2*, a dual-luciferase activity assay was conducted (Figure 7J, K). The addition of either HaMYB120 or HaMYB181 resulted in a significant increase in fluorescence intensity, indicating enhanced regulatory activity on *HaGST3.2*. These results suggest that the interaction among HaMYB22, HaMYB120, and HaMYB181 augments the regulatory effect of HaMYB22 on *HaGST3.2*, thereby enhancing its expression. This interaction appears to play a positive role in modulating plant responses to salt stress.

VIGS of *HaGST3.2* reduces salt tolerance in sunflower

To investigate the function of *HaGST3.2* in sunflower, we generated *HaGST3.2*-silenced plants (Vi: *HaGST3.2*) and treated them with 200 mM NaCl. Initial phenotypic analysis of two-week-old EV and Vi: *HaGST3.2* seedlings indicated that, similar to *HaMYB22*, silencing *HaGST3.2* did not significantly impact normal growth and development (Figure S8).

In both leaves and roots of Vi: *HaGST3.2* plants, *HaGST3.2* expression levels were reduced under both mock and salt treatment, but increased following NaCl exposure, indicating effective silencing and salt-induced expression of *HaGST3.2* (Figures 8A, S9A, B). After 3 h of treatment with 200 mM NaCl, Vi: *HaGST3.2* showed more severe leaf damage compared to EV (Figure 8B). Salt-treated leaves were assessed for damage severity, showing distinct patterns between EV and Vi: *HaGST3.2* (Figure 8C). Vi: *HaGST3.2* had more leaves in higher damage categories (III and IV), indicating greater susceptibility to NaCl stress. Vi: *HaGST3.2* also showed a reduced leaf relative water content (Figure 8D) and increased shrinkage rates (Figure 8E) compared to EV under salt stress, demonstrating that silencing *HaGST3.2* exacerbates salt-induced damage in plants.

Comparative analysis revealed significantly higher MDA content in Vi: *HaGST3.2* after a 3 h salt treatment (Figure 8F). Consistent with this trend, NBT/DAB staining revealed higher ROS accumulation in the leaves and roots of Vi: *HaGST3.2* plants than in the EV under salt stress, which was supported by intensified NBT/DAB staining in Vi: *HaGST3.2* under salt stress (Figure 8G), with quantification using ImageJ software revealing greater superoxide and H_2O_2 accumulation than in EV (Figures 8G, H, S9C, D). Our research showed that silencing *HaGST3.2* also led to increased ROS accumulation in sunflower plants, thereby exacerbating salt stress-induced damage.

These results are consistent with those observed in Vi: *HaMYB22*, collectively indicating that both *HaGST3.2* and *HaMYB22* are involved in regulating ROS homeostasis in roots and leaves under salt stress, and the loss of function of either gene leads to excessive ROS accumulation, thereby supporting the model that they act synergistically within the same signaling pathway.

Allelic variation in *HaMYB22* modulates *HaGST3.2* expression through differential promoter binding

To elucidate the population distribution of *HaMYB22* haplotypes, we analyzed the 135 germplasm accessions and two haplotypes were identified: $HaMYB22^{hap1}$ and $HaMYB22^{hap2}$. A single-nucleotide polymorphism (SNP) was identified between the two haplotypes: an A-to-T substitution at position 271 within the R2R3 domain of $HaMYB22^{hap1}$, resulting in an amino acid change from methionine (Met) at position 90 in $HaMYB22^{hap1}$ to leucine (Leu) in $HaMYB22^{hap2}$ (Figure 9A). Phenotypic analysis revealed significant differences in DW between the haplotypes (Figure 9B), with $HaMYB22^{hap1}$ showing significantly higher DW than $HaMYB22^{hap2}$, indicating that $HaMYB22^{hap1}$ is an agriculturally superior haplotype.

To investigate the molecular mechanism underlying this phenotypic variation, we performed the Y1H assay and found that $HaMYB22^{hap1}$ binds the *HaGST3.2* promoter with significantly higher affinity than $HaMYB22^{hap2}$ (Figure 9C). Meanwhile, compared with $HaMYB22^{hap2}$, $HaMYB22^{hap1}$ showed significantly reduced transcriptional activation efficiency on *HaGST3.2* (Figure 9D, E). Taken together, these findings collectively establish $HaMYB22^{hap1}$ as the elite haplotype with enhanced binding and transcriptional activation activity toward *HaGST3.2*.

DISCUSSION

Our results demonstrate that silencing either *HaMYB22* or *HaGST3.2* in sunflower significantly compromised plant salt tolerance. Both Vi: *HaMYB22* and Vi: *HaGST3.2* showed reduced RWC (Figures 3D, 8D) and accelerated leaf wilting rate (Figures 3E, 8E) compared to EV. This reduced tolerance likely stems from impaired ROS scavenging capacity, as evidenced by significantly elevated MDA levels (Figures 3F, 8F) and ROS accumulation (Figures 3G, H, 8G, H) in Vi: *HaMYB22* and Vi: *HaGST3*. These biochemical alterations ultimately resulted in compromised plant adaptation to saline environments. Molecular analyses revealed that HaMYB22 directly activates the expression of *HaGST3.2* (Figure 7A–G). Studies in various plants have shown that MYB transcription factors can activate the expression of *GST* genes by recognizing MYB-binding sites (MBSs) (Jiang et al., 2019; Zhao et al., 2020). In addition, MYB transcription factors modulate salt tolerance by regulating ROS levels through other mechanisms. In rice, OsMYB2 enhances salt tolerance in rice seedlings by reducing ROS accumulation through elevated antioxidant enzyme activities and proline content (Nie et al., 2025a). MdMYB44 enhances apple salt tolerance by suppressing *MdPP2CA* to potentiate ABA signaling and reduce ROS accumulation

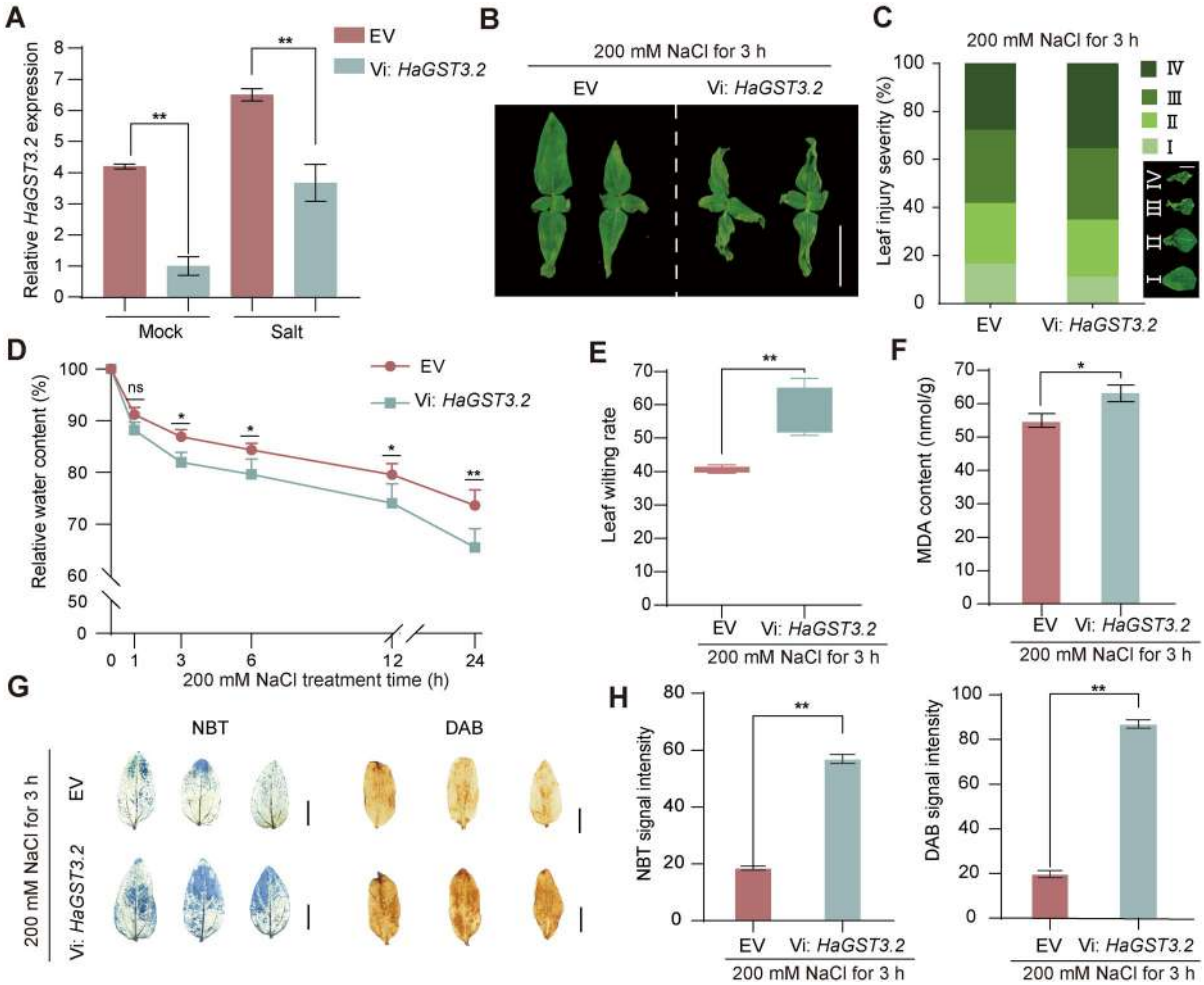

Figure 8. Silencing of *HaGST3.2* decreases salt tolerance in sunflower

(A) Relative expression levels of *HaGST.3.2* in empty vector (EV) and *HaGST3.2*-silenced (Vi: *HaGST3.2*) sunflower seedlings under both untreated (mock) and salt-stressed (200 mM NaCl, 3 h) conditions after 14 d of culture. *HaTubulin* was used as the endogenous control. ($n = 3$, $^{*}P < 0.05$, $^{**}P < 0.01$; Student's *t*-test). **(B, C)** Representative phenotypes **(B)** and quantitative assessment of salt-induced leaf damage **(C)** in EV and Vi: *HaGST3.2* lines after 3 h of 200 mM NaCl treatment (Scale bar = 2.5 cm). Two-week old seedlings cultured in 1/5 Hoagland liquid medium were subjected to 200 mM NaCl stress in identical medium. Tissue deterioration was classified into four severity categories (I: intact → IV: necrotic). Statistical comparisons of leaf damage between EV and Vi: *HaGST3.2* were conducted post-treatment. **(D)** RWC from detached leaves of EV and Vi: *HaGST.3.2* after 200 mM NaCl treatment ($n = 12$, $^{*}P < 0.05$, $^{**}P < 0.01$; Student's *t*-test). Whole-seedling fresh weight was recorded at designated time points (1, 3, 6, 12, and 24 h) after salt exposure to facilitate the calculation of RWC. **(E)** Leaf wilting rate determined as the ratio of pre-treated to post-treated leaf area, in EV and Vi: *HaGST.3.2* plants, after 3 h of 200 mM NaCl treatment ($n = 12$, $^{**}P < 0.01$; Student's *t*-test). **(F)** MDA content of EV and Vi: *HaGST.3.2* under 200 mM NaCl treatment for 3 h ($n = 3$, $^{**}P < 0.01$; Student's *t*-test). **(G–H)** Representative histochemical detection **(G)** and quantification **(H)** of superoxide (NBT) and hydrogen peroxide (DAB) levels in EV and Vi: *HaGST3.2* plants following a 3 h exposure to 200 mM NaCl (Scale bar = 1.0 cm, $n = 12$, $^{**}P < 0.01$; Student's *t*-test).

(Chen et al., 2024). These findings reveal the sophisticated mechanism of MYB-regulating salt tolerance in crop. Protein interaction assays showed that HaMYB120 and HaMYB181 physically interact with HaMYB22 (Figure 6), while dual-luciferase assays further demonstrated their synergistic enhancement of HaMYB22-mediated transcriptional activation of the *HaGST3.2* promoter (Figure 7H). These findings establish a regulatory module where HaMYB120 and HaMYB181 coordinately up-regulate *HaGST3.2* expression through interaction with HaMYB22, playing essential roles in sunflower's adaptation to salt stress.

Based on these findings, we propose a model illustrating how the HaMYB22–HaGST3.2 module enhances plant salt tolerance. In wild-type plants, high NaCl concentrations in saline-alkali soil promote the accumulation of HaMYB22 in the nucleus. HaMYB22 then directly binds to the *HaGST3.2* promoter, activating its transcription with the aid of HaMYB120 and HaMYB181 (Figure 10). Increased HaGST3.2 reduces the excessive accumulation of ROS in plants. However, when this pathway is impaired, limited ROS scavenging leads to excessive accumulation of ROS. In *HaMYB22*-OE plants, increased nuclear levels of HaMYB22 drive even stronger upregulation of *HaGST3.2*, leading to more efficient ROS detoxification. This enhanced activity alleviates salt stress-induced damage and significantly enhances plant salt tolerance.

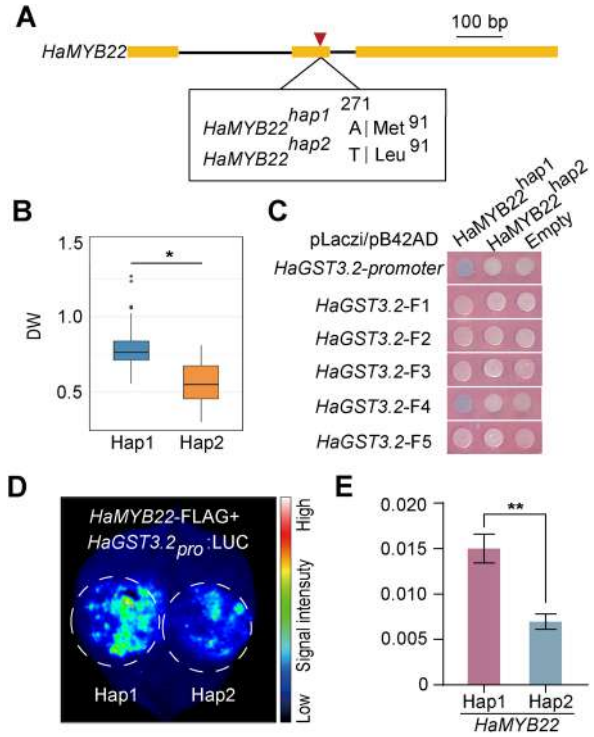

Figure 9. Identification and molecular functional analysis of *HaMYB22* haplotypes

(A) Single-nucleotide polymorphism (SNP) variation between the two haplotypes of *HaMYB22*. The lead SNP A/T in the second exon of *HaMYB22* causes an amino acid substitution from methionine (M) to leucine (L). **(B)** Significance analysis of dry weight (DW) between two haplotypes ($n = 135$, $^{*}P < 0.05$; Student's *t*-test). **(C)** Y1H analysis demonstrated distinct binding affinities between the two HaMYB22 haplotypes to the *HaGST3.2*. **(D)** Transient expression assays using the dual-luciferase reporter system demonstrated the differential regulation of the *HaGST3.2* promoter by two *HaMYB22* haplotypes. **(E)** Relative luciferase activity of two HaMYB22 haplotypes to *HaGST3.2*. Reporter activity (firefly LUC) was normalized to the internal control (Renilla REN) for quantification ($n = 4$, $^{**}P < 0.01$; Student's *t*-test).

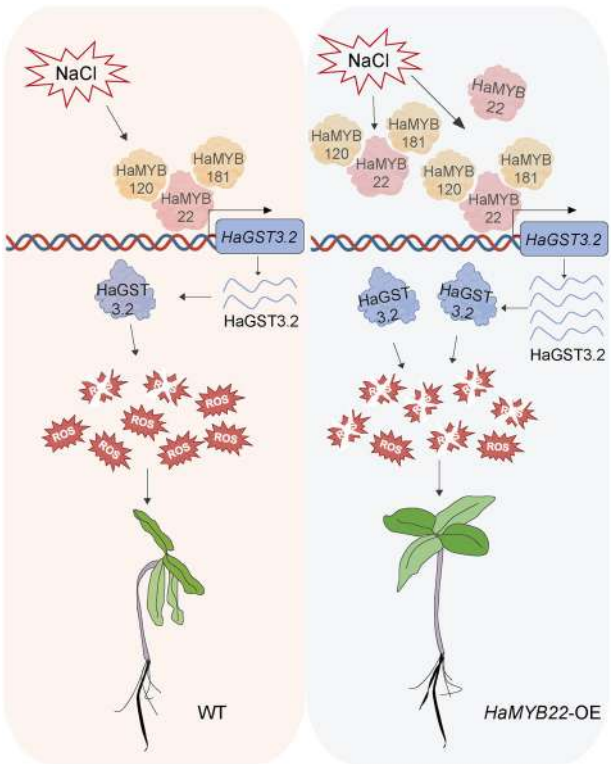

Figure 10. Proposed model for the role of the HaMYB22–HaGST3.2 module in regulating sunflower salt stress tolerance

In wild-type plants (left), salt stress-induced HaMYB22 activates *HaGST3.2* transcription through promoter binding, with this activation being further enhanced by the cooperative action of HaMYB120 and HaMYB121. However, the limited ROS-scavenging capacity of induced HaGST3.2 proteins results in oxidative damage in plants. In *HaMYB22*-overexpressing lines (right), elevated HaMYB22 robustly upregulates *HaGST3.2* expression, enabling more efficient ROS detoxification that significantly enhances plant salt tolerance.

The Y1H results demonstrated that the SNP in *HaMYB22*^{hap2} impaired its DNA-binding capacity, leading to significantly weaker interaction with both the full-length *HaGST3.2* promoter and the key regulatory F4 region (Figure 9C). Consistently, the dual-luciferase reporter assay demonstrated that *HaMYB22*^{hap1} shows significantly stronger transactivation of the *HaGST3.2* promoter than *HaMYB22*^{hap2} (Figure 9D, E). These molecular findings correlate well with the agronomic performance data of the haplotypes. Quantitative analysis revealed a 25% reduction in *HaMYB22*^{hap2}-mediated activation of *HaGST3.2* (Figure 9B), further supporting *HaMYB22*^{hap1} as the elite haplotype. Different haplotypes can significantly affect key agronomic traits in crops, such as yield and disease resistance (Wang et al., 2023; Li et al., 2025; Liu et al., 2025). Therefore, SNP markers specific to *HaMYB22*^{hap1} should be developed to screen germplasm resources carrying this haplotype. These markers will support backcross breeding programs, enhancing research on the utilizing *HaMYB22* in sunflower salt tolerance breeding.

The trade-off between plant growth/development and stress resistance is essential for crop growth due to energy distribution (Kempel et al., 2011; Karasov et al., 2017). Traditional crop breeding has primarily focused on optimizing agronomic trait performance under ideal conditions (Sato et al., 2016). This also explains why cultivated crops show reduced stress resistance compared to their wild ancestors, with many resistance alleles having been lost during domestication and improvement. The reduced frequency of the ZmSRO1d-R allele during maize breeding demonstrates a trade-off between yield and stress resistance, where increased grain productivity may come at the expense of drought tolerance (Gao et al., 2022). The observed expansion with diminished diversity of disease resistance genes in cultivated rice genomes likely stems from the loss of specific resistance genes during domestication (Long et al., 2024). Traits and alleles negatively correlated with crop performance in high-resource environments are most susceptible to elimination by artificial selection (Todesco et al., 2010; Gao et al., 2019), while others may be randomly lost due to domestication bottleneck effects (Hübner et al., 2019; Janzen et al., 2019). In our study, silencing of *HaMYB22*

and *HaGST*3.2 in sunflower did not compromise seedling growth and development (Figures S2, S8). Therefore, these genes hold particular promise for breeding programs aiming to develop cultivars that combine both stress tolerance and maintained yield potential.

Through transcriptomic analysis under salt stress conditions, we identified five strongly salt-responsive MYB family genes in sunflower (Figure 6A, B). Notably, except for *HaMYB22*, the other four *HaMYBs* were not detected in previous GWAS analyses or salt stress transcriptome screenings, suggesting that these genes may not have been selected during sunflower domestication. A natural variation in the *SlSOS2* promoter region in tomato affects root Na^+/K^+ ratio and correlates with salt tolerance loss during domestication (Hong et al., 2023). Our results corroborate with the *SlSOS2* promoter polymorphism, collectively evidencing that contemporary crop improvement programs might have unintentionally lost certain stress-tolerant alleles during yield-oriented domestication. The domestication-retained allele of *HaMYB22* presents a rare instance of dual functionality, influencing both stress adaptation and yield potential in a manner relevant to crop improvement. This finding suggests their immediate applicability in agricultural production for creating sunflower varieties with dual advantages of salt tolerance and stable yield performance. Heterologous expression of sunflower-derived *HaWRKY76* in *Arabidopsis thaliana* confers dual resistance to drought and flooding stress without compromising reproductive yield (Raineri et al., 2015). This unique combination not only provides a natural blueprint for developing salt-tolerant cultivars without compromising yield but also establishes a framework for 'intelligent' breeding strategies. Through the precise identification and utilization of such pleiotropic regulatory genes, we may overcome the persistent yield–stress resistance trade-off that characterizes conventional breeding paradigms. Meanwhile, further validation through stable genetic transformation and field trials remains essential to confirm these findings.

MATERIALS AND METHODS

Genome-wide association study

The GWAS was conducted with the mixed linear model (MLM) that took population structure (Q-matrix) and kinship (*K*-matrix) into account, which was implemented in GEMMA software (https://github.com/genetics-statistics/GEMMA) (Zhou and Stephens, 2012). To determine the significant cutoff for GWAS results, we calculated the genome-wide effective SNPs number using GEC software (https://pmglab.top/gec/). After pruning, a total of 46,408 SNPs were determined as the effective SNP and we then selected 1.08×10^{-6} (Benjamini–Hochberg FDR < 0.05) as the genome-wide significant cutoff. Furthermore, genes located within the linkage disequilibrium (LD) regions of significant SNPs were identified as candidate genes influencing the traits. Genome-wide LD decay analysis was performed using popLDdecay software to calculate pairwise SNP LD levels. The physical distance at which r^2 decayed to 0.2 was considered as the final genome-wide LD decay distance. Genes with associated SNP were selected as the candidate genes.

Plant materials and stress treatment

The sunflower inbred line AZB was used in this study. Uniform, healthy seeds were surface-sterilized and germinated on moist filter paper for 3–5 d. Germinated seedlings were transferred to hydroponic containers with 1/5 Hoagland nutrient solution and cultivated under controlled conditions: 28°C, 40%–60% relative humidity, and a 16 h light/8 h dark photoperiod. For salt stress treatments, EV and gene-silencing materials were exposed to 200 mM NaCl in 1/5 Hoagland solution, whereas EV and gene-overexpressing materials were treated with 300 mM NaCl. Phenotypic responses were documented photographically and quantified at regular intervals. All experiments included three independent biological replicates, with each replicate consisting of 10–12 plants per treatment group.

Arabidopsis Columbia (Col-0) served as the wild-type control in this study. Seeds were surface-sterilized and stratified at 4°C, and then sown onto MS medium at pH 5.8 (Phyto Technology, Cat. M519) with 0.6% (w/v) agar for germination or with 1.2% (w/v) agar for seedling growth. Seedlings were cultivated under controlled conditions with a 16 h light/8 h dark photoperiod at 23°C. For salt stress assays, 7-day-old seedlings grown on MS medium were transferred to 1/2MS medium supplemented with varying NaCl concentrations (0, 90, and 150 mM). Phenotypic responses were monitored daily and quantitatively assessed at 10 d post-treatment. Whole-plant images were acquired using a standardized setup, with root parameters analyzed using ImageJ software. All experiments included at least three independent biological replicates, with 15 seedlings per replicate.

RNA isolation and real-time PCR validation

Total RNA was isolated from mature leaves, roots, and shoots using an RNA Plant Plus Reagent Kit (Tiangen, Cat. DP432). RNA integrity was verified by agarose gel electrophoresis and spectrophotometric analysis. First-strand cDNAs were synthesized using HiScript II Q RT SuperMix (Vazyme, Cat. R223). Quantitative Real-time PCR assay was performed on the CFX384 real-time system (BIO-RAD) with ChamQ Universal SYBR qPCR Master Mix kit (Vazyme, Cat. Q711). At least three biological and technical replicates were fulfilled for each gene. Gene-specific primers used for amplification are listed in Table S2. Relative gene expression levels were calculated using the $2^{-\Delta\Delta Ct}$ method with *HaTubulin* as the internal reference gene.

Generation of *Arabidopsis* transgenic plants

For heterologous expression studies, the coding sequence of *HaMYB22* (LOC110873753) was cloned into binary vectors to generate the *Pro35S:HaMYB22-FLAG* and *Pro35S:HaMYB22-*

GFP constructs. These constructs were transformed into *Agrobacterium tumefaciens* strain GV3101 and subsequently transformed into wild-type *Arabidopsis thaliana* (Col-0 ecotype) using the floral dip method (Clough and Bent, 1998).

Yeast one-hybrid and yeast two-hybrid assays

For the yeast one-hybrid assay, the full coding sequence of *HaMYB22* was cloned into the pB42AD vector, while the full-length and truncated fragments of the *HaGST3.2* promoter were inserted into the pLacZi vector. Plasmid pairs were co-transformed into yeast strain EGY48, following the manufacturer's protocol (Coolaber, Cat. SK2400), with pB42AD empty vector combinations serving as negative controls. Transformants were selected on SD/−Ura/−Trp medium (Coolaber, Cat. PM2260), and subsequently screened on selection plates containing raffinose, galactose, and 80 mg/L X-β-gal (5-Bromo-4-chloro-3-indolyl-β- D-galactopyranoside). β-Galactosidase activity was assessed after a 12 h incubation at 30°C.

For the yeast two-hybrid assay, the coding sequences of *HaMYB2* (LOC110864474), *HaMYB22* (LOC110873753), *HaMYB120* (LOC110917164), *HaMYB173* (LOC110936424), and *HaMYB181* (LOC110939761) were cloned into both pGADT7 and pGBKT7 vectors. All constructs were first tested for autoactivation by co-transforming pGBKT7-MYB constructs with empty pGADT7 into yeast strain AH109 and plating on SD/−Trp/−Leu medium (Coolaber, Cat. PM2220). Transformants were then grown on SD /−Ade/−His/−Leu/−Trp/ plates (Coolaber, Cat. PM2110) for protein interaction selection. Additionally, we generated N-terminal constructs containing the R2R3 DNA-binding domain fused to pGBKT7. The primers used in these assays are listed in Table S3.

Dual-luciferase assays

The coding sequences of *HaMYB2*, *HaMYB22*, *HaMYB120*, *HaMYB173,* and *HaMYB181* were cloned into pCAMBIA1300-nLUC and pCAMBIA1300-cLUC vectors to generate N-terminal and C-terminal luciferase fusion constructs, respectively. The primers used in this assay are listed in Table S3. All recombinant plasmids were verified by sequencing before transformation into *Agrobacterium tumefaciens* strain EHA105. For transient expression assays, bacterial cultures were grown to $OD_{600} = 0.8$ at 28°C with shaking. Equal volumes of cultures containing nLUC and cLUC constructs were mixed and infiltrated into young leaves of 4-week-old *Nicotiana benthamiana* plants using a needleless syringe. After 48 h incubation, infiltrated leaves were sprayed with 1 mM D-luciferin (Promega, E1601) and dark-adapted for 5 min. Luminescence signals were captured using a Lumazone imaging system (FM204813) with a 5 min exposure time. Firefly luciferase (LUC) activity was normalized to Renilla luciferase (REN) activity to account for variation in transformation efficiency. Three independent biological replicates were performed.

Transient luciferase assay

The coding sequences of *HaMYB2*, *HaMYB120*, *HaMYB173,* and *HaMYB181* were cloned into pEarleyGate 202 (N-FLAG) to yield effector constructs. The primers used in this assay are listed in Table S3. For the reporter plasmid, a 2-kb promoter fragment from *HaGST3.2* was inserted into the destination vector pGreenII0800-LUC to create the reporter *HaGST3.2pro:* LUC. The empty pEarleyGate 202 vector served as the negative control. Transient expression assays were performed as previously described.

Subcellular localization

The full-length coding sequence of *HaMYB22* was cloned into the transit expression vector pCAMBIA1305GFP. The primers used in this assay are listed in Table S3. To determine the subcellular localization of HaMYB22, transient expression assays were performed in both sunflower protoplasts and young leaves of *N. benthamiana*. For sunflower protoplast preparation, mesophyll protoplasts were isolated from 2-week-old sunflower leaves using enzymatic digestion (1.5% cellulase R10 and 0.4% macerozyme R10 in 0.4 M mannitol). Protoplasts were transfected with 20 μg of plasmid DNA via polyethylene glycol (PEG)-mediated transformation. For leave infiltration, young leaves of 4-week-old plants were infiltrated with Agrobacterium suspensions carrying the fusion construct. GFP fluorescence was visualized using a Zeiss LSM710 confocal laser scanning microscope. D53-mCherry was used as a nucleus marker.

Histochemical detection of reactive oxygen species

For detection of hydrogen peroxide (H_2O_2) and superoxide ($O_2^{\bullet -}$) accumulation, leaves from 200 mM and 300 mM NaCl-treated sunflower leaves and 150 mM NaCl-treated Arabidopsis roots were harvested for histochemical staining as previously described, with a slight modification (Nan et al., 2019). DAB staining was performed by soaking root samples and vacuum-infiltrating leaf samples with 1 mg/mL DAB (Sigma–Aldrich, D8001) solution for 15 min and subsequently incubated in the staining solution for 12–16 h at 25°C in the dark. For NBT staining, parallel samples were treated with 1 mg/mL NBT (Sigma-Aldrich, N6876) solution following the same protocol. After incubation, the DAB and NBT solution were discarded and anhydrous ethanol was added until chlorophyll was completely removed. Stained areas were quantified from digital images using ImageJ software. For DCFH DA staining, Arabidopsis root samples were incubated in a 5 μm DCFH DA working staining solution (Solarbio, China) for 30 min, followed by thorough washing with anhydrous ethanol to remove residual stain. The treated samples were then observed and imaged using a laser confocal microscope.

Generation of virus-mediated gene silencing and transient overexpression in sunflower

Silencing of *HaMYB22* and *HaGST3.2* was performed using the TRV-based VIGS system as previously described, with a slight modification (Krenek et al., 2015). Unique 280 bp (*HaMYB22*) and 240 bp (*HaGST3.2*) were amplified and cloned into the pTRV2 vector. The recombinant pTRV2 constructs and the pTRV1 helper plasmid were transformed into the GV3101 strain. Bacterial cells cultured to $OD_{600} = 0.8$ were collected and re-suspended with infiltration buffer. Sunflower seed coats were

removed after 48 h water imbibition, and the inner epidermis was carefully excised. Uniform wounds were created on both cotyledonary surfaces using sterile forceps. Wounded seeds were immersed in the prepared bacterial suspension for 4–6 h and vacuum-infiltrated three times for 5 min. Seeds were surface-dried and incubated in Petri dishes lined with moist filter paper for 3–5 d at 26°C before transfer to 1/5 Hoagland nutrient solution. Silencing efficiency was verified by RT-qPCR 14-day post-infiltration, with three biological replicates.

Sunflower seedlings cultivated in 1/5 Hoagland nutrient solution were infected at the two-leaf stage. *Agrobacterium* suspensions containing *HaMYB22*-FLAG and the GFP empty vector (used as a control with similar size) were placed in an appropriate container; uniformly sized sunflower seedlings were selected with all leaves immersed in the infection solution. After vacuum infiltration of leaves, seedlings were transferred to 1/5 Hoagland solution for continued cultivation under light conditions after infection. After 2–3 d, a subset of samples was collected to assess infection efficiency, while the remaining materials were subjected to NaCl treatment for phenotypic observation and statistical analysis.

Electrophoretic mobility shift assay

The full-length sequence of *HaMYB22* was cloned into the pMAL-c2X vector. The MBP-tag fusion constructs were transformed into expression strain BL21 (DE3) for protein production as described (Ling et al., 2025). The MBP–HaMYB22 fusion protein was purified according to the manufacturer's protocol using amylose resin (NEB, e8021s). The protein concentration was determined using the Bradford assay. For probe preparation, an 80 bp *HaGST3.2* promoter region containing the predicted MYB-binding motif was divided into two overlapping fragments. Biotinylated double-stranded DNA probes were synthesized by BGI company and annealed in annealing buffer. EMSA was performed using the LightShift Chemiluminescent EMSA Kit (Thermo, 20148) according to the instructions provided by the manufacturer.

Pull-down assay

To verify the interaction between HaMYB22 and HaMYB120/HaMYB181 *in vitro*, the coding sequence of HaMYB22 was constructed into the pMAL-c2X vector containing a MBP tag, while HaMYB120 and HaMYB181 were constructed into the pGEX-4T-1 vector containing a GST tag. These constructs were then transformed into *E. coli* BL21(DE3) cells as described (Li et al., 2019). The successfully induced proteins were subjected to pull-down assays using BeyoMag™ His magnetic beads (Beyotime, Cat. P2239) according to the manufacturer's protocol.

Data availability statement

The RNA-sequencing raw data have been deposited in the Sequence Read Archive at the National Center for Biotechnology Information (http://www.ncbi.nlm.nih.gov/sra) under accession number PRJNA1417350.

ACKNOWLEDGEMENTS

This research was supported by Leading Talent of Science and Technology Innovation of Xinjiang Province (2024TSYCLJ0045), the Interdisciplinary Research Project of Hangzhou Normal University (2025JCXK01), The Starting Research Fund from Hangzhou Normal University (2019QDL015), and Tianchi Talents Program of Xinjiang Province (YHBH01003732). The authors thank Prof. Hada Wuriyanghan (Inner Mongolia University) for kindly providing us with TRV plasmids and Prof. Xian Zhang (Hangzhou Normal University) for assistance with tobacco growth.

CONFLICTS OF INTEREST

The authors declare no conflicts of interest.

AUTHOR CONTRIBUTIONS

S.Z. performed most of the experiments, analyzed the data, and drafted the manuscript. Q.H and Y.H. provided technical assistance. W.G. and S.D. performed the GWAS analysis. Y.H., X.L., and Q.Z. collected the samples and worked on the phenotyping. J.Z., Y.M., and Z.L. revised the manuscript. M.C. and T.C. designed and supervised this study. All authors provided final approval for publication.

Edited by: Caifu Jiang, China Agricultural University, China

Received Sept. 17, 2025; **Accepted** Jan. 20, 2026; **Published** Feb. 17, 2026

OO: OnlineOpen

REFERENCES

Badouin, H., Gouzy, J., Grassa, C.J., Murat, F., Staton, S.E., Cottret, L., Lelandais-Brière, C., Owens, G.L., Carrère, S., Mayjonade, B., et al. (2017). The sunflower genome provides insights into oil metabolism, flowering and Asterid evolution. Nature **546:** 148–152.

Bhatt, P.A., Gurav, T.P., Kondhare, K.R., and Giri, A.P. (2025). MYB proteins: Versatile regulators of plant development, stress responses, and secondary metabolite biosynthetic pathways. Int. J. Biol. Macromol. **288:** 138588.

Chen, C., Zhang, Z., Lei, Y.Y., Chen, W.J., Zhang, Z.H., Li, X.M., and Dai, H.Y. (2024). MdMYB44-like positively regulates salt and drought tolerance via the MdPYL8-MdPP2CA module in apple. Plant J. **118:** 24–41.

Chen, Q., Liu, R., Wang, Q., and Xie, Q. (2017). ERAD Tuning of the HRD1 complex component AtOS9 is modulated by an ER-Bound E2, UBC32. Mol. Plant **10:** 891–894.

Clough, S.J., and Bent, A.F. (1998). Floral dip: A simplified method for *Agrobacterium*-mediated transformation of *Arabidopsis thaliana*. Plant J. **16:** 735–743.

Gagliardi, D., Cambiagno, D.A., Arce, A.L., Tomassi, A.H., Giacomelli, J.I., Ariel, F.D., and Manavella, P.A. (2019). Dynamic regulation of chromatin topology and transcription by inverted repeat-derived small RNAs in sunflower. Proc. Natl. Acad. Sci. U.S.A. **116:** 17578–17583.

Gao, H., Cui, J., Liu, S., Wang, S., Lian, Y., Bai, Y., Zhu, T., Wu, H., Wang, Y., Yang, S., et al. (2022). Natural variations of *ZmSRO1d* modulate the trade-

off between drought resistance and yield by affecting ZmRBOHC-mediated stomatal ROS production in maize. Mol. Plant **15:** 1558–1574.

Gao, L., Lee, J.S., Hübner, S., Hulke, B.S., Qu, Y., and Rieseberg, L.H. (2019). Genetic and phenotypic analyses indicate that resistance to flooding stress is uncoupled from performance in cultivated sunflower. New Phytol. **223:** 1657–1670.

Gao, L.J., Liu, X.P., Gao, K.K., Cui, M.Q., Zhu, H.H., Li, G.X., Yan, J.Y., Wu, Y.R., Ding, Z.J., Chen, X.W., et al. (2023). ART1 and putrescine contribute to rice aluminum resistance via OsMYB30 in cell wall modification. J. Integr. Plant Biol. **65:** 934–949.

Giacomelli, J.I., Weigel, D., Chan, R.L., and Manavella, P.A. (2012). Role of recently evolved miRNA regulation of sunflower HaWRKY6 in response to temperature damage. New Phytol. **195:** 766–773.

Gill, S.S., and Tuteja, N. (2010). Reactive oxygen species and antioxidant machinery in abiotic stress tolerance in crop plants. Plant Physiol. Biochem. **48:** 909–930.

Gong, Q., Li, S., Zheng, Y., Duan, H., Xiao, F., Zhuang, Y., He, J., Wu, G., Zhao, S., Zhou, H., et al. (2020). SUMOylation of MYB30 enhances salt tolerance by elevating alternative respiration via transcriptionally upregulating *AOX1a* in Arabidopsis. Plant J. **102:** 1157–1171.

Hadidi, M., Aghababaei, F., and McClements, D.J. (2024). Sunflower meal/cake as a sustainable protein source for global food demand: Towards a zero-hunger world. Food Hydrocoll. **147:** 109329.

Harter, A.V., Gardner, K.A., Falush, D., Lentz, D.L., Bye, R.A., and Rieseberg, L.H. (2004). Origin of extant domesticated sunflowers in eastern North America. Nature **430:** 201–205.

Hong, Y., Guan, X., Wang, X., Kong, D., Yu, S., Wang, Z., Yu, Y., Chao, Z.F., Liu, X., Huang, S., et al. (2023). Natural variation in *SlSOS2* promoter hinders salt resistance during tomato domestication. Hortic. Res. **10:** uhac244.

Hübner, S., Bercovich, N., Todesco, M., Mandel, J.R., Odenheimer, J., Ziegler, E., Lee, J.S., Baute, G.J., Owens, G.L., Grassa, C.J., et al. (2019). Sunflower pan-genome analysis shows that hybridization altered gene content and disease resistance. Nat. Plants **5:** 54–62.

Janzen, G.M., Wang, L., and Hufford, M.B. (2019). The extent of adaptive wild introgression in crops. New Phytol. **221:** 1279–1288.

Jiang, S., Chen, M., He, N., Chen, X., Wang, N., Sun, Q., Zhang, T., Xu, H., Fang, H., Wang, Y., et al. (2019). *MdGSTF6*, activated by MdMYB1, plays an essential role in anthocyanin accumulation in apple. Hortic. Res. **6:** 40.

Karasov, T.L., Chae, E., Herman, J.J., and Bergelson, J. (2017). Mechanisms to mitigate the trade-off between growth and defense. Plant Cell **29:** 666–680.

Kempel, A., Schädler, M., Chrobock, T., Fischer, M., and Kleunen, M.V. (2011). Tradeoffs associated with constitutive and induced plant resistance against herbivory. Natl. Acad. Sci. USA. **108:** 5685–5689.

Kotula, L., Caparros, P.G., Zörb, C., Colmer, T.D., and Flowers, T.J. (2020). Improving crop salt tolerance using transgenic approaches: An update and physiological analysis. Plant Cell Environ. **43:** 2932–2956.

Krenek, P., Samajova, O., Luptovciak, I., Doskocilova, A., Komis, G., and Samaj, J. (2015). Transient plant transformation mediated by *Agrobacterium tumefaciens*: Principles., methods and applications. Biotechnol. Adv. **33:** 1024–1042.

Lapenna, D. (2023). Glutathione and glutathione-dependent enzymes: From biochemistry to gerontology and successful aging. Ageing Res. Rev. **92:** 102066.

Leconte, J.M.L., Moroldo, M., Blanchet, N., Bindea, G., Carrère, S., Catrice, O., Comar, A., Labadie, M., Marandel, R., Pouilly, N., et al. (2025). Multi-scale characterization of cold response reveals immediate and long-term impacts on cell physiology up to seed composition in sunflower. Plant Cell Environ. **48:** 2596–2614.

Li, N., Lin, B., Wang, H., Li, X., Yang, F., Ding, X., Yan, J., and Chu, Z. (2019). Natural variation in *ZmFBL41* confers banded leaf and sheath blight resistance in maize. Nat. Genet. **51:** 1540–1548.

Li, S., Liu, G., Wu, Z., Zhang, D., Gan, C., Li, B., Liu, J., Ni, Z., Sun, Q., and Liang, R. (2025). The TaMYB44-TaMYB1 module regulates grain amylose biosynthesis and flour viscosity in wheat. Plant Commun. **6:** 101461.

Liang, X., Li, J., Yang, Y., Jiang, C., and Guo, Y. (2024). Designing salt stress-resilient crops: Current progress and future challenges. J. Integr. Plant Biol **66:** 303–329.

Ling, C., Yang, J., Xu, J., Tang, W., Liu, Y., Wang, Y., Li, P., He, Y., Ouyang, Z., Chen, S., et al. (2025). Natural variation of *AcEGY3* mediates chloroplastic ROS homeostasis to confer kiwifruit thermotolerance. Nat. Commun. **16:** 6184.

Liu, H., Li, J., He, Y., Zheng, T., Lin, H., Xu, C., Zhang, Q., Ye, Y., Lin, C., and Shen, Z. (2024). Characterization of transgenic insect resistant sunflower (*Helianthus annuus* L.). expressing fusion protein Cry1Ab-Vip3Af2. Int. J. Biol. Macromol. **281:** 136219.

Liu, Y., Zhang, S., Li, J., Muhammad, A., Feng, Y., Qi, J., Sha, D., Hao, Y., Li, B., and Sun, J. (2025). An R2R3-type MYB transcription factor., GmMYB77., negatively regulates isoflavone accumulation in soybean [*Glycine max* (L.). Merr.]. Plant Biotechnol. J. **23:** 824–838.

Long, W., He, Q., Wang, Y., Wang, Y., Wang, J., Yuan, Z., Wang, M., Chen, W., Luo, L., Luo, L., et al. (2024). Genome evolution and diversity of wild and cultivated rice species. Nat. Commun. **15:** 9994.

Lv, J., Liang, D., Bumann, E., Mirleau, T., Thebaud, V., Jin, H., Li, C., Paris, C., Dan, Y., Li, C., et al. (2025) Haploid facultative parthenogenesis in sunflower sexual reproduction. Nature **641:** 732–739.

Manavella, P.A., Arce, A.L., Dezar, C.A., Bitton, F., Renou, J.P., Crespi, M., and Chan, R.L. (2006). Cross-talk between ethylene and drought signalling pathways is mediated by the sunflower Hahb-4 transcription factor. Plant J. **48:** 125–137.

Mittler, R. (2017). ROS are good. Trends Plant Sci. **22:** 11–19.

Mittler, R., Zandalinas, S.I., Fichman, Y., and Breusegem, F.V. (2022). Reactive oxygen species signaling in plant stress responses. Nature **23:** 663–679.

Munns, R., and Tester, M. (2008). Mechanisms of salinity tolerance. Annu. Rev. Plant Biol. **59:** 651–681.

Nan, N., Wang, J., Shi, Y., Qian, Y., Jiang, L., Huang, S., Liu, Y., Wu, Y., Liu, B., and Xu, Z. (2019). Rice plastidial NAD-dependent malate dehydrogenase 1 negatively regulates salt stress response by reducing the vitamin B6 content. Plant Biotechnol. J. **18:** 172–184.

Nanda, A.K., Andrio, E., Marino, D., Pauly, N., and Dunand, C. (2010). Reactive oxygen species during Plant-microorganism early interactions. J. Integr. Plant Biol **52:** 195–204.

Nie, S., Huang, W., He, C., Wu, B., Duan, H., Ruan, J., Zhao, Q., and Fang, Z. (2025a). Transcription factor OsMYB2 triggers amino acid transporter OsANT1 expression to regulate rice growth and salt tolerance. Plant Physiol. **197:** kiae559.

Raineri, J., Caraballo, L., Rigalli, N., Portapila, M., Otegui, M.E., and Chan, R.L. (2022). Expressing the sunflower transcription factor HaHB11 in maize improves waterlogging and defoliation tolerance. Plant Physiol. **189:** 230–247.

Raineri, J., Ribichich, K.F., and Chan, R.L. (2015). The sunflower transcription factor HaWRKY76 confers drought and flood tolerance to *Arabidopsis thaliana* plants without yield penalty. Plant Cell Rep. **34:** 2065–2080.

Renaut, S. (2017). Genome sequencing: Illuminating the sunflower genome. Nat. Plants **3:** 17099.

Russell, T.M., and Richardson, D.R. (2023). The good samaritan glutathione-S-transferase P1: An evolving relationship in nitric oxide metabolism mediated by the direct interactions between multiple effector molecules. Redox Biol. **59:** 102568.

Sato, H., Todaka, D., Kudo, M., Mizoi, J., Kidokoro, S., Zhao, Y., Shinozaki, K., and Shinozaki, K.Y. (2016). The Arabidopsis

transcriptional regulator DPB3-1 enhances heat stress tolerance without growth retardation in rice. Plant Biotechnol. J. **14:** 1756–1767.

Smith, B.D. (2006). Eastern North America as an independent center of plant domestication. Proc. Natl. Acad. Sci. U.S.A. **103:** 12223–12228.

Sun, Y., Tian, Z., Zuo, D., Wang, Q., and Song, G. (2024). GhUBC10-2 mediates GhGSTU17 degradation to regulate salt tolerance in cotton (*Gossypium hirsutum*). Plant Cell Environ. **47:** 1606–1624.

Sun, Y., Zhao, J., Li, X., and Li, Y. (2020). E2 conjugases UBC1 and UBC2 regulate MYB42-mediated SOS pathway in response to salt stress in Arabidopsis. New Phytol. **227:** 455–472.

Temme, A.A., Kerr, K.L., Masalia, R.R., Burke, J.M., and Donovan, L.A. (2020). Key traits and genes associate with salinity tolerance independent from vigor in cultivated sunflower. Plant Physiol. **184:** 865–880.

Todesco, M., Balasubramanian, S., Hu, T.T., Traw, M.B., Horton, M., Epple, P., Kuhns, C., Sureshkumar, S., Schwartz, C., Lanz, C., et al. (2010). Natural allelic variation underlying a major fitness trade-off in *Arabidopsis thaliana*. Nature **465:** 632–636.

Wang, J., Nan, N., Li, N., Liu, Y., Wang, T.J., Hwang, I., Liu, B., and Xu, Z.Y. (2020). A DNA methylation reader–chaperone regulator–transcription factor complex activates *OsHKT1;5* expression during salinity stress. Plant Cell **32:** 3535–3558.

Wang, P., Liu, W.C., Han, C., Wang, S., Bai, M.Y., and Song, C.P. (2024). Reactive oxygen species: Multidimensional regulators of plant adaptation to abiotic stress and development. J. Integr. Plant Biol. **66:** 330–367.

Wang, T., Jin, Y., Deng, L., Li, F., Wang, Z., Zhu, Y., Wu, Y., Qu, H., Zhang, S., Liu, Y., et al. (2023). The transcription factor MYB110 regulates plant height., lodging resistance., and grain yield in rice. Plant Cell **36:** 298–323.

Waszczak, C., Carmody, M., and Kangasjärvi, J. (2018). Reactive oxygen species in plant signaling. Annu. Rev. Plant Biol. **69:** 209–236.

Wu, X., Xia, M., Su, P., Zhang, Y., Tu, L., Zhao, H., Gao, W., Huang, L., and Hu, Y. (2024). MYB transcription factors in plants: A comprehensive review of their discovery., structure., classification., functional diversity and regulatory mechanism. Int. J. Biol. Macromol. **282:** 136652.

Wu, Y., Wen, J., Xia, Y., Zhang, L., and Du, H. (2022). Evolution and functional diversification of R2R3-MYB transcription factors in plants. Hortic. Res. **9:** uhac058.

Xu, R., Wang, Y., Zheng, H., Lu, W., Wu, C., Huang, J., Yan, K., Yang, G., and Zheng, C. (2015). Salt-induced transcription factor MYB74 is regulated by the RNA-directed DNA methylation pathway in Arabidopsis. J. Exp. Bot. **66:** 5997–6008.

Yang, Y., and Guo, Y. (2018). Elucidating the molecular mechanisms mediating plant salt-stress responses. New Phytol. **217:** 523–539.

Yuan, L., Dang, J., Zhang, J., Wang, L., Zheng, H., Li, G., Li, J., Zhou, F., Khan, A., Zhang, Z., et al. (2024). A glutathione S-transferase regulates lignin biosynthesis and enhances salt tolerance in tomato. Plant Physiol. **196:** 2989–3006.

Zhang, D., Zhou, H., Zhang, Y., Zhao, Y., Zhang, Y., Feng, X., and Lin, H. (2025). Diverse roles of MYB transcription factors in plants. J. Integr. Plant Biol. **67:** 539–562.

Zhang, H., Zhu, J., Gong, Z., and Zhu, J.K. (2022a). Abiotic stress responses in plants. Nat. Rev. Genet. **23:** 104–119.

Zhang, Y., Ming, R., Khan, M., Wang, Y., Dahro, B., Xiao, W., Li, C., and Liu, J.-H. (2022b). ERF9 of *Poncirus trifoliata* (L.). Raf. undergoes feedback regulation by ethylene and modulates cold tolerance via regulating a *glutathione S-transferase U17* gene. Plant Biotechnol. J. **20:** 183–200.

Zhao, Y., Dong, W., Zhu, Y., Allan, A.C., Wang, K.L., and Xu, C. (2020). *PpGST1*, an anthocyanin-related glutathione S-transferase gene., is essential for fruit coloration in peach. Plant Biotechnol. J. **18:** 1284–1295.

Zhou, X., and Stephens, M. (2012). Genome-wide efficient mixed-model analysis for association studies. Nat. Genet. **44:** 821–824.

Zhu, J.K. (2016). Abiotic stress signaling and responses in plants. Cell **167:** 313–324.

SUPPORTING INFORMATION

Additional Supporting Information may be found online in the supporting information tab for this article: http://onlinelibrary.wiley.com/doi/10.1111/jipb.70184/suppinfo

Figure S1. Validation of *HaMYB22* overexpression efficiency in *Arabidopsis* transgenic lines

Figure S2. Seedling phenotypes of plant growth and development in EV and Vi: *HaMB22*

Figure S3. Analysis of ROS accumulation in roots of EV and Vi: *HaMB22* plants under salt stress

Figure S4. Analysis of ROS accumulation in roots of EV and *HaMYB22*-OE plants under salt stress

Figure S5. Identification and interaction network analysis of salt-responsive HaR2R3–MYB transcription factors

Figure S6. Self-activation verification of five HaMYB proteins

Figure S7. Identification and cis-element promoter analysis of downstream target genes regulated by HaMYB22

Figure S8. Seedling phenotype of plant growth and development in EV and Vi: *HaGST3.2*

Figure S9. Analysis of ROS accumulation in roots of EV and Vi: *HaGST3.2* plants under salt stress

Table S1. Transcriptomic profiling of salt stress response in GWAS candidate genes

Table S2. Primer sequences for RT-qPCR

Table S3. Gene construction primers